Gas-limited Hydrogenation of 1-Octene in a Packed Bed Reactor

Fritz Reynders

Gas-limited Hydrogenation of 1-Octene in a Packed Bed Reactor

by

Fritz Reynders

A thesis submitted in fulfillment
of the requirements for the subject CVD 800

Master of Engineering (Chemical Engineering)

in the

Department of Chemical Engineering
Faculty of Engineering, the Built Environment and Information Technology

University of Pretoria
Pretoria

July 22, 2011

Gas-limited Hydrogenation of 1-Octene in a Packed Bed Reactor

Author:	Fritz Reynders
Supervisor:	W. Nicol
Department:	Department of Chemical Engineering University of Pretoria
Degree:	Master of Engineering (Chemical Engineering)

Synopsis

A 1-octene hydrogenation reaction was studied under gas-limited conditions in a semi-batch laboratory autoclave as well as in a packed bed reactor, in order to better interpret packed bed experimental results. Hydrogen gas solubility in $C_{14} - C_{20}$ paraffin, gas-liquid mass transfer and particle rate kinetics for Pd/Al_2O_3 catalyst were measured in the autoclave reactor.

Most significant autoclave experimental findings include:

- Hydrogen solubility (He) at 60 ℃, was measured as 2.2 $^{mole}/_{m^3.bar}$ and was found to be independent of pressure in the experimental pressure range of 3 - 6 bar
- Very low gas-liquid mass transfer coefficients were measured at stirrer speeds below 1000 rpm, and exponential increase was observed above this critical velocity ($k_{GL}a \propto N^{5.3}$)
- Langmuir-Hinshelwood kinetics best fitted rate data, with the best model corresponding to a mechanism with dissociative non-competitive adsorption of H_2 and weak adsorption of the alkene

Three different operational modes were compared in the packed bed reactor, including two differently prewetted co-current downflow modes as well as co-current upflow of gas and liquid. Packed bed and autoclave experimental work was limited to temperatures between 40 and 60 ℃, total pressure of < 9 bar (p_{H_2} between 0.9 and 4 bar) as well as packed bed liquid and gas velocities of below 5.5 and 16 $^{mm}/_{s}$ respectively.

The traditional hypothesis that gas-limited reactions favour downflow operation because of fractional dry surface area was not confirmed. Although downflow outperformed upflow in some experiments (higher gas densities), conversions of extensively prewetted downflow always exceeded that of Levec prewetted (known to have lower wetting efficiencies). Higher gas mass velocities favoured downflow operation, suggesting that

a hydrodynamic flow regime inhibiting effect occurred during upflow rather than a dry area enhancing effect during trickle flow. Hydrodynamic modeling confirmed that reactions were gas-liquid mass transfer limited, and slugging in the upflow mode considerably decreased gas-liquid mass transfer.

Because Packed bed reactions were gas-liquid mass transfer driven, $k_{GL}a$ values were fitted to experimental data as the only unknown. For upflow no definite trend was observed regarding $k_{GL}a$, while for downflow data was correlated by $k_{GL}a \approx 7.7\frac{P_{tot}}{M_G}v_L^{0.35}$ and $k_{GL}a \approx 8.8\frac{P_{tot}}{M_G}v_L^{0.35}$ for Levec and extensively prewetted beds respectively. The inconsistency of fitted $k_{GL}a$ values for upflow is indicative of a hydrodynamic flow regime shift during this flow configuration, which is most likely responsible for the observed performance variations.

During packed bed reaction comparative studies (up- vs. downflow), a priori hydrodynamic regime verification for the entire experimental range is recommended in order to decouple fractional wetting effects from flow effects that are regime dependent. It is concluded from experimental work that upflow outperforms downflow even under gas-limited conditions when operated in a homogeneous bubbling regime because of higher gas-liquid and liquid-solid mass transfer rates.

KEYWORDS: packed bed reactor, gas-limited reactions, hydrogenation, rate kinetics, upflow, trickle flow

NOMENCLATURE

α	Variable used in equation 2.13	-
β	Ratio of $\frac{D_{H_2}}{D_{OCT}}$	-
ϵ	Bed porosity defined as void fraction of packed bed	-
$\frac{\Delta P}{\Delta Z}$	Pressure drop per unit bed length	$^{\mathrm{Pa}}/_{\mathrm{m}}$
γ	Reactant limitation criterion, $= \frac{D_{e,A} C_{A,bulk}}{b D_{e,B} C_B^*}$	-
λ	Dimensionless parameter defined in equation 4.1	-
μ_i	Viscosity of substance/phase i	$\mathrm{Pa} \cdot \mathrm{s}$
ϕ	Particle sphericity	-
ψ	Dimensionless parameter defined in equation 4.2	-
ρ_i	Density of substance/phase i	$^{\mathrm{kg}}/_{\mathrm{m}^3}$
σ_i	Surface tension of substance/phase i	$^{\mathrm{mN}}/_{\mathrm{m}}$
θ_i	Fractional coverage of catalyst active sites by component i	-
a_{LS}	Liquid-solid mass transfer area per volume of packing	m^{-1}
b	Stoichiometric factor for gas reactant reacting with liquid reactant	-
$C_{i,s}$	Surface concentration of substance i	$^{\mathrm{mole}}/_{\mathrm{L}}$
C_i	Concentration of component i	$^{\mathrm{mole}}/_{\mathrm{L}}$
D_{AB}	Molecular diffusivity of component A in B	$^{\mathrm{m}^2}/_{\mathrm{s}}$

D_c	Column diameter	m
$D_{e,i}$	Effective diffusivity of reactant i	$^{m^2}/_{s}$
d_p	Particle diameter	m
d_t	Impeller blade diameter	m
Fr_i	Froude number of phase i, $= \frac{v_i^2}{gd_p}$	-
G	Gas mass flux	$^{kg}/_{m^2 \cdot s}$
g	Gravitational acceleration	$^{m}/_{s^2}$
H_t	Total liquid holdup per volume of reactor	-
He	Henry's law constant	$^{mole}/_{L.bar}$
$k_{GL}a$	Overall volumetric liquid-side gas-liquid mass transfer coefficient	s^{-1}
K_i	Quasi-equilibrium adsorption constant of reaction i, $= \frac{k_i}{k_{-i}}$	$^{L}/_{mole}$
k_i	Rate constant of surface reaction i	Reaction dependant
k_{LS}	Liquid-solid mass transfer coefficient	$^{m}/_{s}$
L	Liquid mass flux	$^{kg}/_{m^2 \cdot s}$
l	Packed bed reactor length	m
N	Stirrer speed	rpm
P_0	Liquid phase degassed equilibrium pressure	kPa
P_f	Final reactor pressure after gas absorption	kPa
p_i	Partial pressure of gas i	bar
P_m	Pressure before agitation is started for gas absorption to begin	kPa
R	Ideal gas constant	$^{kJ}/_{kmole \cdot K}$
r_i	Rate of reaction of species i	$^{mole}/_{L.s}$
Re_L	Liquid Reynolds number, $= \frac{\rho_L v_L d_p}{\mu_L}$	–
Re_t	Turbine Reynolds number, $= \frac{N\rho_L d_t^2}{\mu_L}$	-
Sc_L	Liquid Scmidt number, $= \frac{\mu_L}{\rho_L D_{AB}}$	–

T	Reactor temperature	℃
v_G	Gas superficial velocity	$^{m}/_{s}$
V_i	Volume of phase i	m^3
v_L	Liquid superficial velocity	$^{m}/_{s}$
We	Weber number, $=\frac{\rho_L v_L^2 d_p}{\sigma_L H_t^2}$	-
X	Dimensionless parameter defined in equation 4.6	-
X_i	Mole fraction of substance i in the liquid phase	-
Y	Dimensionless parameter defined in equation 2.4	-

CONTENTS

LIST OF FIGURES

LIST OF TABLES

CHAPTER 1

INTRODUCTION

Packed bed reactors (PBRs) are are commonly used for multiphase reactions where both a gas and a liquid reagent are processed on a solid catalyst. The gas reagent first dissolves into the liquid phase (gas-liquid mass transfer), before both reagents in the liquid phase diffuse to the catalyst active sites for reaction (liquid-solid mass transfer). Besides these mass transfer mechanisms, which are hydrodynamic flow regime specific, reaction rates are also affected by catalyst kinetics. The operating regime becomes more significant when a reaction is limited by the rate of external mass transfer, because regime flow effects determines the gas-liquid contacting effectiveness. To achieve succesful commercialization of a specific reaction process, good understanding of both particle-scale and reactor-scale behaviour is required and should be integrated (van Houwelingen, 2009: 2).

PBRs are extensively utilized in the petrochemical industry for hydroprocessing, oil refining and biochemical processes (Gianetto & Specchia, 1992: 3197). PBRs can be operated with countercurrent flow, co-current downflow and co-current upflow of liquid and gas. The latter two flow configurations are more often used for industrial processes. Trickle bed reactors (TBRs) refer to fixed beds of catalyst contacted by co-current downflow of gas and liquid, and packed bubble columns (PBCs) operate with two phases flowing co-currently upward. Due to the flexibility in terms of throughput of TBRs, this flow configuration is often preferred when large process streams are involved. PBCs are used less frequently on industrial scale but are utilized in laboratory scale reactors for testing catalyst and alternative feed stocks (Khadilkar et al., 1996: 2139).

Besides catalysis, hydrodynamic differences between various flow regimes can have a considerable effect on reactor performance of both up- and downflow configurations. The choice of up- or downflow configuration is a question as old as research on fixed bed multiphase reactors. The obvious difference between the two modes is the extent of external wetting. PBCs also typically exhibit higher interphase mass transfer rates

than TBRs at the same operating conditions (Gianetto & Specchia, 1992). Downflow operation at relatively low superficial velocities is known for partial wetting of catalyst particles. This was initially believed to be a drawback because the entire external surface area is not available for mass transfer (Goto & Smith, 1975: 21), which slows down the overall transport of reactants to the active sites. This idea was contradicted by various authors who found that downflow outperformed upflow operation at the same liquid and gas superficial velocities (Goto & Mabuchi (1984), Beaudry et al. (1987) and Goto et al. (1993)).

Their results were explained with the concept of a limiting reagent. A reagent is limiting when the catalyst is starved of that reagent, and consequently its rate of mass transfer controls the global reaction rate. The overall rate of mass transfer of the gaseous reactant is believed to be enhanced by a direct gas-solid mass transfer step if particles are partially dry (Khadilkar et al., 1996). This enhancement effect is thought to cause downflow (known for partial wetting) to outperform upflow when the gas reactant is limiting. Khadilkar et al. (1996) was the first to define a criterion, the so called γ-factor, to distinguish between gas and liquid limitation. The γ-factor is calculated with molecular diffusion, bulk liquid and saturated gas concentrations, and accounts for internal and external diffusional effects. Khadilkar also compared up- and downflow performance at two sets of H_2 partial pressures and liquid feed concentration, and related reactor performance to the limitation criteria.

Hydrodynamic differences between up- and downflow packed beds are not limited to the extent of external wetting, but external mass transfer steps also result in performance variations. In this regard it is convenient to employ an additional hydrodynamic steady state during trickle flow, in order to extend the conventional up-down analysis to a study with two different downflow modes. Different wetting efficiencies can be obtained in a TBR under the same operating conditions depending on the flow history and prewetting procedure (van der Merwe & Nicol, 2008: 249). By comparing two downflow modes with different wetting efficiencies to fully wetted upflow, more light can be shed on possible reasons for observed rate differences.

Besides different wetting efficiencies, the degree of gas-limitation must also be considered. The effects of operational mode on a PBRs performance are well documented in the literature, and a summary of a few of them can be found in an article by Khadilkar et al. (1996: 2144). However, very few of these studies were done at different liquid concentrations and gas reactant partial pressures with a constant gas mass flux. This approach allows one to vary the extent of reactant limitation while operating in the same hydrodynamic regime. This technique was utilized in this study because it enables one to compare up- and downflow performance with minimal flow variations, for different degrees of reactant limitation. This study is consequent to previous work on the same reactor setup for liquid-limited conditions (van Houwelingen & Nicol (2009)).

A 1 m long 50 mm inside diameter PBR was used at gas-limited conditions for three different operational modes; upflow, extensively prewetted and Levec prewetted trickle flow. In addition to the packed bed experiments, a 450 ml Parr 4843 autoclave reactor was used to determine particle kinetics which facilitated the modelling of the PBR. The reaction of concern is 1-octene hydrogenation. The liquid phase consisted of dilute 1-octene in a $C_{14} - C_{20}$ paraffin solvent, and the catalyst used was 3 mm γ-Pd/Al_2O_3 eggshell spheres with a 0.3% (by weight) Pd loading.

CHAPTER 2

LITERATURE

2.1 Packed Bed Reactor Hydrodynamics

In all applications of multiphase packed bed reactors (PBRs), knowledge of fluid dynamics and transport parameters are necessary for the development of a reactor model and scale-up (Dudukovic et al., 1999: 1975). Catalytic PBRs have been studied extensively because of their commercial importance, especially during the last two decades (Gianetto & Specchia (1992); Al-Dahhan et al. (1997); Dudukovic et al. (1999)). Many publications discuss mass transfer, partial wetting, holdup and pressure drop, but with a level of contradictory results. The following subsections discuss these factors relevant to practical reactor design. The aim was to comparatively summarize hydrodynamic aspects for up- and downflow operation of PBRs most likely responsible for performance discrepancies between these two flow modes. This would in turn enable one to better comprehend why specific flow configurations (up- vs. downflow) favour reactions with specific reactant limitations (liquid vs. gas reactant limiting).

2.1.1 Flow Regimes

The complex flow behaviour in multiphase PBRs results in various flow regimes, each with a different extent of phase interaction (high and low interaction regimes). Hydrodynamic parameters differ extensively for different flow regimes while the transition boundaries between regimes are usually gradual and difficult to predict (Dudukovic et al., 1999: 1997). It is well known that trickle bed reactors (TBRs) and packed bubble columns (PBCs) can operate in various flow regimes with unique hydrodynamic charactaristics. Although PBRs with co-current downflow of gas and liquid are termed trickle bed reactors (TBRs), trickle flow is just one of various flow regimes encountered in these type of

reactors. Flow regimes in TBRs include the following (Dudukovic et al., 1999: 1977):

- Spray or mist flow - at low liquid and high gas flow rates, fine liquid droplets are dispersed and entrained by a continuous gas current
- Trickle flow - at relatively low liquid and low to moderate gas flow rates, liquid rivulets and some discontinuous liquid films occur. A continuous gas phase slips through spaces unoccupied by liquid. The term trickle-bed (TBR) is often used for co-current downflow packed beds, even when they are not operated in the trickling regime.
- Pulse flow - average to very high gas and liquid flow rates are charactarized by intermittent passage of gas- and liquid-rich zones
- Downward bubble flow - at high liquid and low gas flow rates, a continuous liquid phase forms with dispersed bubbles. This regime is fairly uncommon to industrial reactors (Trambouze & Euzen, 2004: 504).

Although the existence of these flow regimes have been proven, criteria proposed in the literature to delineate the regime boundaries are not entirely successful (Dudukovic et al., 1999: 1977). A general consensus classifies these regimes into two broad regimes, namely, a low interaction regime (LIR; trickle flow) and high interaction regime (HIR; pulse, spray and bubble flow).

The most important regime boundary considered in downflow operation is probably the trickle-to-pulse transition, because industrial reactors typically operate in the vicinity of this regime transition with v_L and v_G often limited to 3 and 30 cm/s respectively (Trambouze & Euzen, 2004: 505). Al-Dahhan et al. (1997) summarized empirical trickle-to-pulse boundary correlations and theoretical models from various researchers to predict trickle-pulse regime transition. Regime mappings from different authors for co-current downflow packed beds coincide and correspond well, and a generally accepted regime map is shown in figure 2.1.

Here λ and ψ are corrective parameters that are functions of the liquid and gas properties, and account for variations in fluid properties (equations 4.1 and 4.2):

$$\lambda = \sqrt{\frac{\rho_G \rho_L}{\rho_{air} \rho_{water}}} \tag{2.1}$$

$$\psi = \frac{\sigma_{water}}{\sigma_L} \left(\frac{\mu_L \rho_{water}}{\mu_{water} \rho_L} \right)^{1/3} \tag{2.2}$$

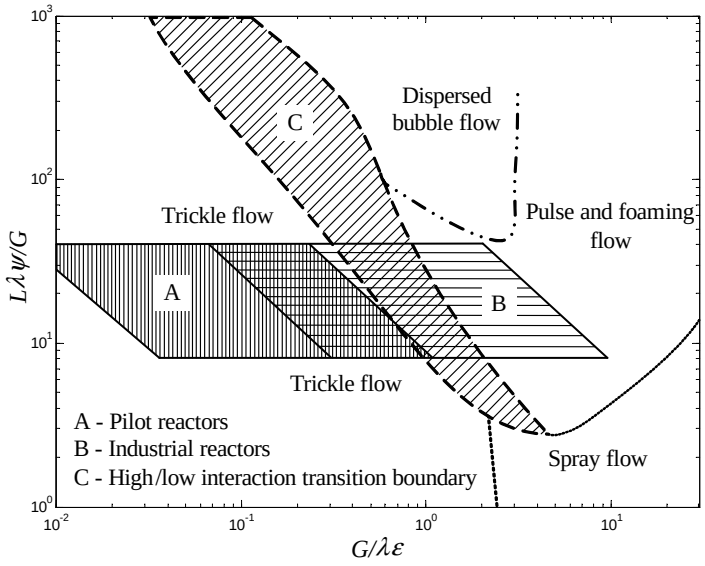

Figure 2.1: Regime mapping for TBRs (Gianetto & Specchia, 1992)

Charpentier (1976) presented flow patterns in terms of mass velocities for various gases and foaming hydrocarbon systems (figure 2.2), as well as for non-foaming systems. They showed the influence of foaming hydrocarbons on reactor performance, and have also taken gas density into account to compensate for pressure effects. Foaming in a TBR drastically influences gas-liquid mass transfer in the form of interfacial area, as well as lower wetting efficiency. A priori prediction of foaming still remains elusive (Dudukovic et al., 1999: 1979).

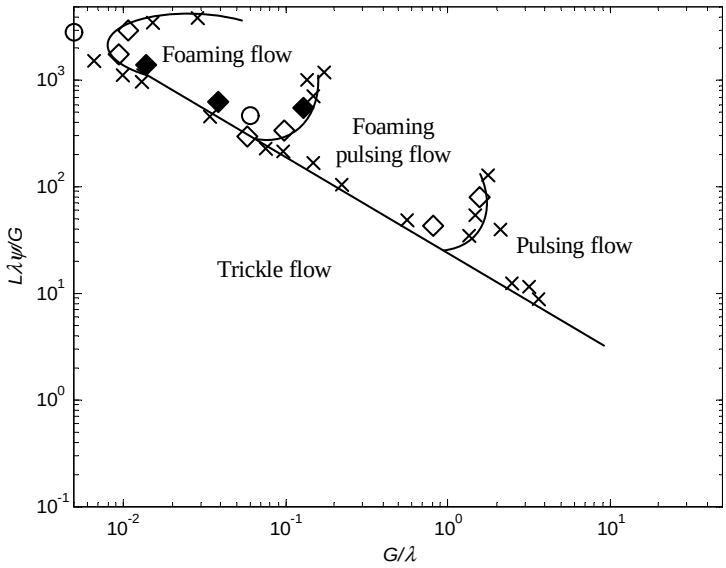

Figure 2.2: Regime mapping for foaming liquids in TBRs (Charpentier, 1976)

Upflow multiphase reactors are used less frequently than TBRs, and consequently our understanding of them is limited. The change in fluid circulation direction appreciably alters hydrodynamic charactaristics. PBCs have also been observed to operate in various flow regimes depending on the fluid properties, flow rates and packing charactaristics (Dudukovic et al., 1999: 1979):

- Homogeneous bubbling flow - uniform size bubbles in a continuous liquid phase occurs when gas flow rates are fairly low, especially when packing size is $\gtrsim$ 4 mm (Trambouze & Euzen, 2004: 519)
- Heterogeneous bubbling flow - tiny and larger bubbles exist within a continuous liquid phase
- Slugging/pulsed flow - at high gas flow rates ($G \gtrsim 0.01 - 1^{kg}/_{m^2 s}$), high liquid and gas content pulses flow through the bed
- Spray/mist flow - This regime occurs as with TBRs, and is encountered less frequently

The regime diagram (figure 2.3) effectively explains regime transition by means of liquid and gas flow rate alterations.

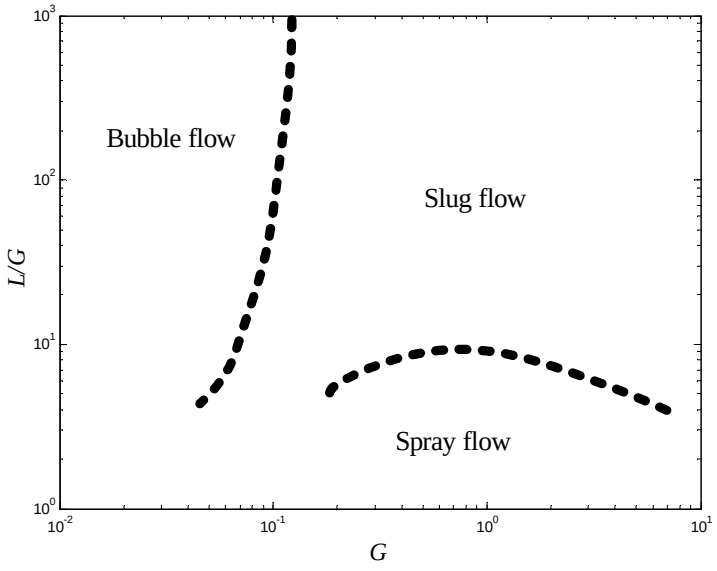

Figure 2.3: Regime mapping for PBCs (Gianetto & Specchia, 1992)

Because upflow reactors are used comprehensively for catalyst testing, knowledge on interphase contacting efficiency for different flow regimes is required because it is regime specific. The regime map in figure 2.3 has satisfactorily represented experimental data from various authors (Gianetto & Specchia, 1992: 3199). Murugesan & Sivakumar

(2002: 238) summarized a further 8 regime maps for upflow through packed beds, and most of them coincide well. In their work, they also developed a regime map that corrects for fluid property differences, and takes into account the reactor and packing properties (figure 2.4). In the following sections hydrodynamic parameters for up- and downflow are discussed and compared.

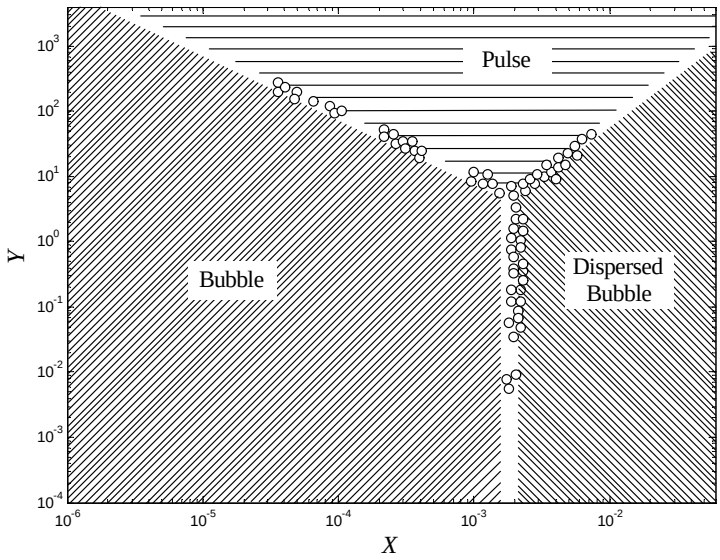

Figure 2.4: Regime mapping for PBCs (Murugesan & Sivakumar, 2002)

Here X and Y are given by equations 4.6 and 2.4:

$$X = Fr_L \left(\frac{d_p}{D_c}\right) \epsilon^{-1} \psi \tag{2.3}$$

$$Y = \frac{\left(\frac{Fr_G}{Fr_L}\right)\left(\phi \frac{d_p}{D_c}\right)^{0.75} \epsilon^{-1}}{\psi} \tag{2.4}$$

2.1.2 Gas-liquid Mass Transfer

In three phase gas-liquid-solid systems such as TBRs, gas-liquid mass transfer resistance can have detrimental effects on the overall reactor performance (Al-Dahhan et al., 1997: 3305). The overall gas-liquid mass transfer rate is often assumed to be controlled by the liquid side only, because the gas side coefficient is expected to diminish with increased gas density or low gas solubility (Dudukovic et al., 2002: 160). Accurate estimation of the volumetric liquid side gas-liquid mass transfer coefficient is therefore important for successful reactor design and scale-up.

Although literature exist for both gas-liquid mass transfer coefficients as well as for interfacial area, they are usually lumped as a single volumetric parameter ($k_{GL}a$) because the latter is very difficult to measure on its own. For downflow packed beds,

Al-Dahhan et al. (1997) summarized published literature on gas-liquid interfacial area, mass transfer coefficients and lumped liquid-side volumetric mass transfer coefficients in the trickling regime. The main observations based on these studies are as follows:

- Liquid-side mass transfer coefficients and interfacial areas increase with an increase in liquid mass flux for a given gas density
- For gas superficial velocity less than 1-2 cm/s, neither of these parameters are dependant on gas density
- At gas flow rates more than 1-2 cm/s, these parameters increase with an increase in gas density

The latter effect was interpreted by Cassanello et al. (1996) as a competition between the liquid's viscous shear stress which tends to deform and break the bubbles and the force induced by interfacial tension, which tends to stabilise them. The greater the gas density, the more important the gas shear over the trickling liquid film becomes. The larger the gas shear, the more gas gets entrained into the liquid above the critical velocity and disperses into liquid films forming bubbles. Cassanello et al. (1996) also found the critical velocity to be in the vicinity of 2-3 cm/s.

Regarding the high interaction or pulsing regime, it is apparent that greater gas-liquid shear exists. This greater shear gives rise to better liquid spreading, particle wetting and gas-liquid interfacial area. Reiss (1967) correlated both gas- and liquid-side mass transfer coefficients with individual phase energy dissipation, which is directly related to the two-phase pressure drop per unit bed length. Larger pressure drops occure in the pulsing regime, meaning larger energy dissipation and accordingly gas-liquid mass transfer.

Sylvester & Pitayaguisarn (1975) experimented in the gas-continuous, liquid continuous and pulsing regimes and found the largest gas-liquid mass transfer rates at the flow rates corresponding to pulsing flow. In addition to this, Sylvester & Pitayaguisarn (1975) also found the gas-liquid mass transfer to be a lot less sensitive to gas flow rate at lower liquid velocities. A good comparitive visual representation of $k_{GL}a$ data between high and low interaction downflow was compiled by Gianetto & Specchia (1992). In this work he also compared $k_{GL}a$ for downflow packed beds with that of upflow (figure 2.5).

In upflow configuration a continuous liquid phase forces all of the gas to be dispersed into the liquid in the form of bubbles, in contrast to trickle flow where a continuous gas phase exists. This causes a much larger gas-liquid interfacial area in upflow than downflow configurations. Besides the much larger interfacial area for gas-liquid transport, mass transfer in upflow is much greater due to better axial and radial distribution in comparison with rivulet flow during low interaction downflow (Murugesan & Sivakumar, 2002: 233).

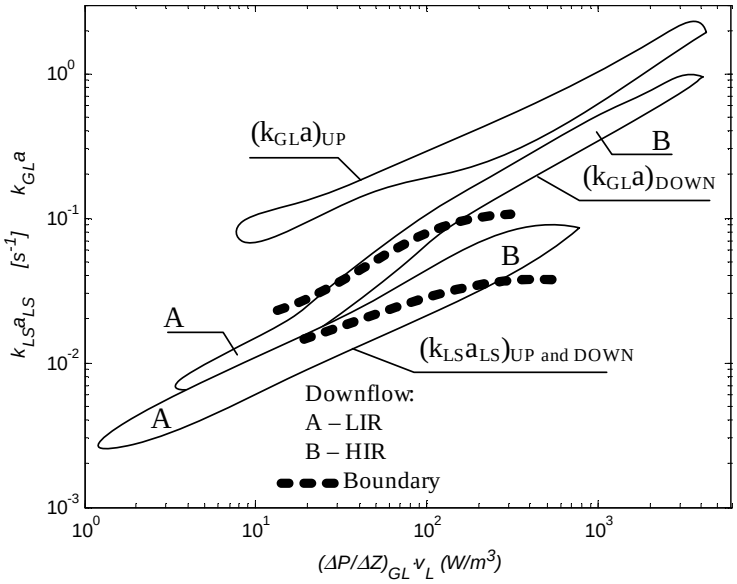

Figure 2.5: $k_{GL}a$ and k_{LS} data comparison for downflow (HIR and LIR) and upflow (Gianetto & Specchia, 1992)

Gianetto & Specchia (1992) performed 210 experiments and compared liquid-controlled volumetric gas-liquid mass transfer rates for LIR and HIR downflow with that of upflow (see figure 2.5). From their results they concluded that $k_{GL}a$ values for upflow are much higher than that of downflow, especially at their lowest operating rates (4-7 times higher) (Gianetto & Specchia, 1992: 3202). Molga & Westerterp (1997) measured interfacial areas by means of a chemical absorption method in PBCs for a wide range of experimental conditions, including bubbling and a maldistributed flow regimes. Some of their most important findings are listed below:

- Reactor pressure has no or little effect on the interfacial area in their experimental range of superficial gas flow rates (1-5 cm/s)
- Interfacial areas increase with an increase in superficial gas velocity
- Flow maldistribution became more prominent with smaller packings and smaller diameter columns were found to have larger interfacial gas-liquid areas.

Regarding upward slug-flow in packed beds, scarcity of literature is probably due to the complex hydrodynamics associated with this regime.

2.1.3 Liquid-Solid Mass Transfer

Liquid-solid mass transfer is usually measured using an electrochemical or dissolution technique, and vast numbers of correlations exist to predict k_{LS} (Dudukovic et al., 2002:

159). These correlations are typically a function of Re_L and Sc_L, and are often under-predicted in TBRs because very few of them compensate for any possible partial wetting enhancement effect (Banchero et al. (2004)). Partial wetting means liquid holdup is less than that of a flooded bed, giving rise to higher interstitial velocities. When reaction-based measurement techniques are used, gas-solid mass transfer becomes an important aspect to consider. Gas-solid mass transfer is usually regarded as instantaneous, and accompanies liquid-solid mass transfer when particles have partially dry areas.

Specchia et al. (1978) measured k_{LS} values and compared it for downflow operation in both high and low interaction regimes. It was found that at constant liquid flow rate, on increasing the gas flow rate, the volumetric mass transfer coefficient $k_{LS}a_{LS}$ increased. This increase was noticeable at low gas velocities and slow at higher gas velocities, tending to a horizontal asymptote at very high gas flow rates. Specchia et al. (1978: 365) found that $k_{LS}a_{LS}$ became independent of v_G at superficial gas velocities of roughly 10 and 40 cm/s for up- and downflow respectively. The rate of increase at low v_G values depends on the packing size and is higher for a lower surface tension to liquid viscosity ratio. The pulsing regime exhibits a similar trend (Specchia et al., 1978: 364). Other researchers have however found the liquid-solid mass transfer rate to be independant of gas flow rate (Goto & Smith (1975) and van Krevelen & Krekels (1948)).

Volumetric $k_{LS}a_{LS}$ also increases drastically with v_L. Partly because of wetting efficiency and partly because of k_{LS} both increasing as the liquid flow rate is raised. At the high interaction conditions when particles are fully wetted, $k_{LS}a_{LS}$ increases at a slower rate because a_{LS} is constant. The main contribution to the increasing effect is then because of an increase in k_{LS} due to increased liquid-solid shear and decreased boundary layer thickness (Specchia et al., 1978: 365). Specchia successfully correlated their data using the Weber number (We), because it takes into account the surface tension and accounts for wetting effects by means of holdup.

Besides wetting and holdup effects, variations in flow structure between differently prewetted beds were also suggested to influence liquid-solid mass transfer charactaristics (van Houwelingen & Nicol, 2009: 8). Joubert & Nicol (2009: 8390) found the specific liquid-solid mass transfer coefficients of a Levec prewetted bed to be lower than that of an extensively prewetted bed at low pressures, despite the higher interstitial velocities encountered for the latter case (lower holdup). This was also confirmed by van Houwelingen & Nicol (2009: 8) in high pressure operation. Their measured k_{LS} values were 10-20 % higher for extensively prewetted than for the Levec-prewetted beds, with only a 2-10 % difference in partial wetting. This is evidence that besides wetting and interstitial velocity differences, flow characteristics also influence liquid-solid mass transfer to a certain extent.

In contrast to the work by Gianetto & Specchia (1992) shown in figure 2.5 where $k_{LS}a_{LS}$ is approximately the same for up- and downflow configurations, Specchia et al.

(1978) found that the rate of liquid-solid mass transfer for upflow to be slightly higher. In their work the ratio $\frac{(k_{LS}a_{LS})_{up}}{(k_{LS}a_{LS})_{down}}$ was found to slightly decrease with an increase in v_G, and to increase almost proportionally to the increase in v_L (figure 2.6).

van Houwelingen (2009: 8) compared up- and downflow liquid-solid mass transfer rates for a liquid-limited reaction system. They observed wetting-based liquid-solid mass transfer coefficients for upflow to be 12-30 % higher than that of downflow, at wetting efficiencies of 90 % and higher. Once again this suggests that the specific (wetting-based) liquid-solid mass transfer during downflow operation is influenced by the flow morphology ((van Houwelingen & Nicol, 2009: 9). The discrepancies in experimental findings regarding up- and downflow comparitive studies for k_{LS} can be attributed to an uncertain a priori flow regime verification.

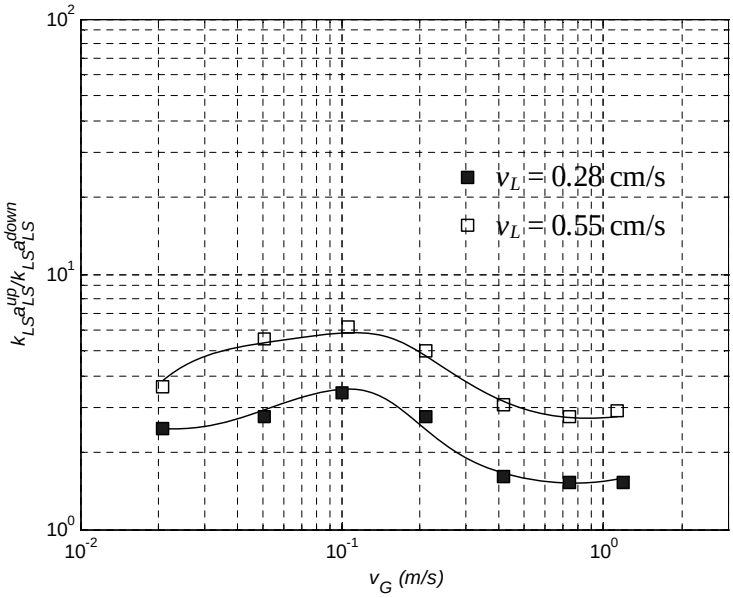

Figure 2.6: Liquid-solid mass transfer ratio for up- and downflow as a function of v_G (Specchia et al., 1978)

2.1.4 Pressure Drop and Liquid Holdup

Because holdup and pressure drop are interdependant and greatly affect wetting efficiency and gas-liquid mass transfer respectively, they are very important in reaction studies. Reactor pressure drop governs the energy required to move fluids through the system, and is therefor important in scale-up and design of reactors (Ellman et al., 1988: 2201). Pressure drop is directly influenced by holdup, because the higher the holdup the more resistance there is to gas flow. The most important trends and aspects regarding pressure drop and holdup are discussed below (Dudukovic et al., 1999: 157):

- At a given gas density, two-phase pressure drop increases with gas and liquid mass

fluxes. H_t however decreses with v_G and gas mass flux, and increases with liquid mass flux and viscosity.

- Both $\frac{\Delta P}{\Delta Z}$ and H_t increase with beds containing fines mixed with the catalyst. This impact is strongly dependant on the packing procedure, and packings with the same void fraction have been shown to result in pressure drops varying by as much as 50 % (Satterfield, 1975: 213).

- For no gas flow, trickle flow has a zero pressure gradient regardless of the pressure. Liquid holdup is also pressure insensitive at $v_G <$ 1-2 cm/s, and equal to the holdup determined at atmospheric conditions.

- At a given set of liquid and gas mass fluxes, $\frac{\Delta P}{\Delta Z}$ increases and H_t decreases with an increase in v_G.

- Pressure drops for different gas mixtures with the same gas densities and liquid flow rates are identical.

- TBRs generally have lower pressure drops than PBCs, and approach that of PBCs in the pulsing regime. PBCs have significantly larger holdups than TBRs which results in unform wetting and thermal homogenity (Trambouze & Euzen, 2004: 522).

Holdup is classified into internal (pore) and external holdup, with the latter further divided into free-draining (dynamic) and residual (static holdup). The residual holdup is typically very low (< 0.05) and a function of the liquid viscosity and particle size, while the free-draining holdup is a function of liquid and gas flow charactaristics as well as the packing properties (Satterfield, 1975: 214). Pressure drop and external liquid holdup also depend on the flow history. For TBRs, an extensively prewetted bed would exhibit greater holdup and pressure drop than a Levec-prewetted bed (van Houwelingen et al., 2006: 3538).

Correlations to predict pressure drop and holdup in the open literature are often biased by wall phenomena (when $^{D_c}/_{d_p} <$ 15-20), and are therefor inaccurate for industrial scale reactors. Illiuta et al. (1999) proposed pressure drop and holdup correlations by means of neural networks from historic flow databases over the last 50 years. They fitted data of 22000 experiments with great accuracy, and would thus provide a comfortable safety margin to predict these parameters for industrial scale reactors (Trambouze & Euzen, 2004: 507).

2.1.5 Wetting

For downflow systems, especially in the trickle flow regime, incomplete catalyst utilization can occur due to partial wetting effects. The two possible causes of incomplete wetting

are reactor-scale liquid maldistribution and particle-scale incomplete wetting. The latter case is encountered when liquid throughput is too low to cover all of the particles with a continuous liquid film at all times (Dudukovic et al., 1999: 161). Reactor-scale wetting effects can be addresed by proper distributor design and packing with minimal pressure drop.

Most correlations used to predict wetting efficiency were obtained from tracer response measurement techniques that depend on the effect of intraparticle diffusion on a tracer response curve. (Kundu & Nigam, 2003) for instance utilized a radioisotope tracer technique. With this technique they measured effective diffusivities during two-phase and liquid-filled operation. Experimental wetting efficiency is measured by the square root of the ratio of these diffusivities. They investigated five different packings with different geometries, and concluded that the wetting efficiency of extrudates and tables etc. is lower than that of spheres due to liquid maldistribution encountered with irregular shaped particles.

Most correlations to predict wetting efficiency were obtained from tracer response measurement techniques, that depend on the effect of intraparticle diffusion on a tracer response curve. Other methods include dissolution (Specchia et al., 1978), colorimetry (van Houwelingen et al., 2006) and reaction methods. The wetting efficiencies measured by van Houwelingen et al. (2006: 3538) with a colorimetric method for Levec and extensively prewetted beds are shown in figure 2.7

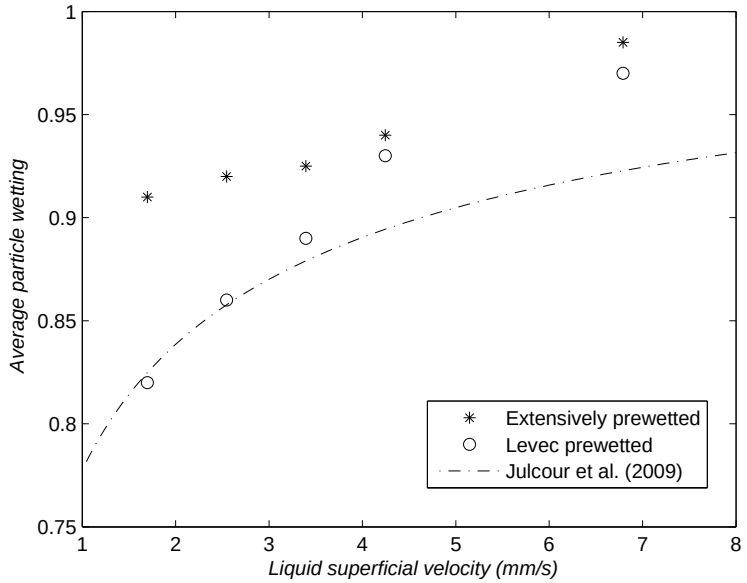

Figure 2.7: Average partial wetting differences for extensively and Levec prewetting procedures (van Houwelingen et al., 2006: 3538)

Particle-scale wetting effects have also been investigated by various other investigators, and the most obvious observations include (Dudukovic et al., 1999: 162):

- At fixed gas and liquid mass fluxes, wetting can be increased by an increase in total system pressure
- Increasing pressure drop and liquid mass flux increases liquid-solid contacting efficiency
- Elevated temperatures may cause decreased partial wetting because of reactant vaporization

Catalyst wetting is an especially important parameter to consider when choosing an operational mode (upflow vs. downflow). Partially wetted conditions is preferred when a reaction is gas-limiting because gas reactant transport to the catalyst is facilited by the dry areas. This emphesizes the significance of prewetting procedure. van Houwelingen et al. (2006) measured particle wetting using a colorimetric method, and concluded that extensively prewetted (Kan-prewetted) beds can have up to 20 % better wetting than a Levec-prewetted bed at similar flow rates. Furthermore, Levec-prewetted beds can contain up to 7 % fraction of unutilized catalyst bed, while Kan-prewetted beds utilize the entire catalyst bed. Perfect wetting is approached at fairly high liquid mass fluxes (about 2 $^{kg}/_{m^2s}$), depending on the gas superficial velocity (Al-Dahhan & Dudukovic, 1995: 2386) and prewetting procedure (higher for Levec).

2.1.6 Liquid distribution

Radial liquid distribution play an important role in determining the reactor performance in a trickle bed reactor. As mentioned in the previous section, liquid maldistribution not only result in poor wetting efficiency but also thermal instability and non-optimal use of the catalyst Kundu et al. (2001).

Various parameters affect the liquid distribution in a trickle bed reactor, and a few effects are summarized below:

- Decrease in liquid density improves liquid distribution efficiency, while wall flow increases with an increase in liquid surface tension
- An increase in liquid flow rate results in better liquid distribution up to a specific liquid flow rate at a given gas mass flux
- Increase in gas flow rate increases the extent of liquid distribution, but its effect is not as prominent as that of liquid flow rate
- Spherical packing particles result in better liquid distribution than irregular shaped particles

In reactor design it is thus important to not only consider the inlet distributor when it comes to radial liquid distribution, but also the reactor operating conditions and fluid properties.

2.2 Reaction Studies: Upflow vs. Downflow

An excellent review of operational mode comparative studies can be found in an article by Khadilkar et al. (1996). In this work they investigated the effect of flow configuration on gas- and liquid-limited hydrogenation of α-methylstyrene using a 2.5 % $Pd\text{-}Al_2O_3$ catalyst, and proposed a single criterion to identify the limiting reactant. Most data in the literature can be explained by the hand of this criterion, and a few are summarized in table 2.1.

Table 2.1: Indication of limiting reactant and preferred operational mode for literature data (Khadilkar et al., 1996: 2144)

Reference	Reaction system	Operating conditions	Gamma (γ)	Limiting reactant	Preferred mode
Goto (1984)	Ethanol oxidation (carbonate present)	Low concentration and P_{atm}	314	gas	downflow
Beaudry (1987)	Hydrogenation of α-methylstyrene	High concentration low pressure	92	gas	downflow
Mazzarino (1989)	Ethanol oxidation	Low concentration and P_{atm}	0.51	liquid	upflow
	Ethanol oxidation	High concentration and P_{atm}	17	gas	downflow
Goto (1993)	Ethanol oxidation (carbonate present)	P_{atm}	10300	gas	downflow
Khadilkar (1996)	α-methylstyrene hydrogenation	High concentration low pressure	8.8	gas	downflow
	α-methylstyrene hydrogenation	Low concentration high pressure	0.87	liquid	upflow

A reaction of $A+bB \rightarrow C$ is classified as gas- or liquid-limited on the basis of γ, where γ is given by equation 3.1. When a reactant is limiting, large concentration gradients of that reactant exist both internally and externally, and its rate of mass transfer controls the overall reaction rate. The γ-criterion is indicative of relative availability of the liquid/gas species at the catalyst active sites, and accounts for external and internal mass transfer effects. A value of $\gamma \gg 1$ would imply a gaseous reactant limitation while $\gamma \ll 1$ indicates liquid reactant limitation. Downflow operation have been confirmed favourable when gas-limited reactions are of concern, believed to be due to a partial wetting enhancement effect that allows gas reactant to directly diffuse on to the catalyst surface. According to the

studies in table 2.1, the opposite holds for liquid-limited reactions which favours upflow with complete catalyst wetting.

$$\gamma = \frac{D_{e,A} C_{A,bulk}}{b D_{e,B} C_B^*} \tag{2.5}$$

Gas-limited cases shown in table 2.1 correspond to γ-values ranging from 8.8 - 10300. Reactions include aqueous ethanol oxidation and α-methylstyrene hydrogenation, and supported Pd catalyst was used in all of these studies. A similar trend was observed regarding preferred operational mode from the gas-limited studies, that is downflow outperforms upflow. Only Khadilkar et al. (1996) and Mazzarino et al. (1989) however investigated both liquid and gas limited instances, and compared reaction rates of upflow and downflow for both cases (figures 2.8 and 2.9).

Several differences were noted in the gas-limited reaction studies from table 2.1. For instance assumptions regarding gas-liquid and liquid-solid mass transfer limitations were different for most of the studies. Goto & Mabuchi (1984) experimentally proved that gas-liquid mass transfer was negligible and ignored liquid-solid mass transfer effects. Beaudry et al. (1987) and Mazzarino et al. (1989) assumed infinite $k_{GL}a$ and k_{LS}, while Khadilkar et al. (1996) estimated k_{GL} and k_{LS} from correlations.

Fractional wetting and flow regime verification by the respective authors were mostly done with the aid of correlations, and only Mazzarino et al. (1989) experimented in two different upflow regimes (bubbling and slugging). They concluded from their experimental work that reaction rates were independant of the flow regime. Furthermore they observed that reaction rates were independant of gas mass flux in the slugging regime, and increased with v_G in the bubbling regime. None of the other studies however observed a flow regime effect on reactor performance, although Beaudry et al. (1987) and Khadilkar et al. (1996) also operated in a possible slug flow regime according to upflow packed bed regime mappings from Gianetto & Specchia (1992).

Khadilkar et al. (1996) determined intrinsic kinetics in a batch slurry reactor to aid in their packed bed reactor analysis, while all other studies obtained kinetics from literature. Similar conclusions were drawn from most of the gas-limited studies regarding the reason why downflow outperformed upflow. The fact that dry catalyst surfaces promotes reaction rates during gas-limited conditions was the general explanation. A direct gas-solid mass transfer step with negligible resistance was incorporated into the reactor models by all authors from the relevant reaction studies, and they all achieved excellent model predictions.

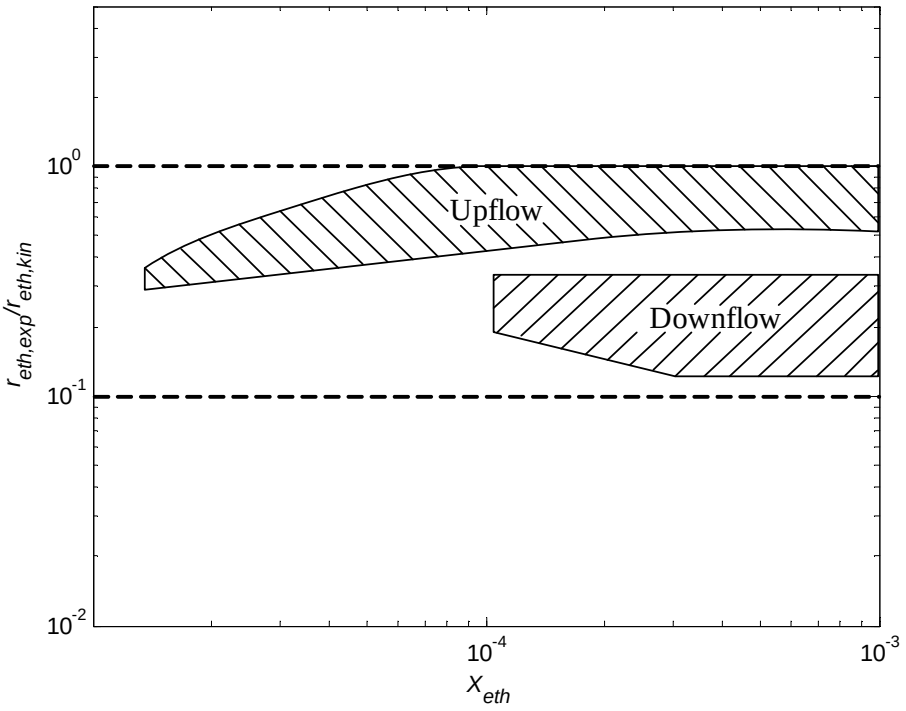

Figure 2.8: Upflow vs. downflow reactor performance for liquid-limited ethanol oxidation (Mazzarino et al., 1989)

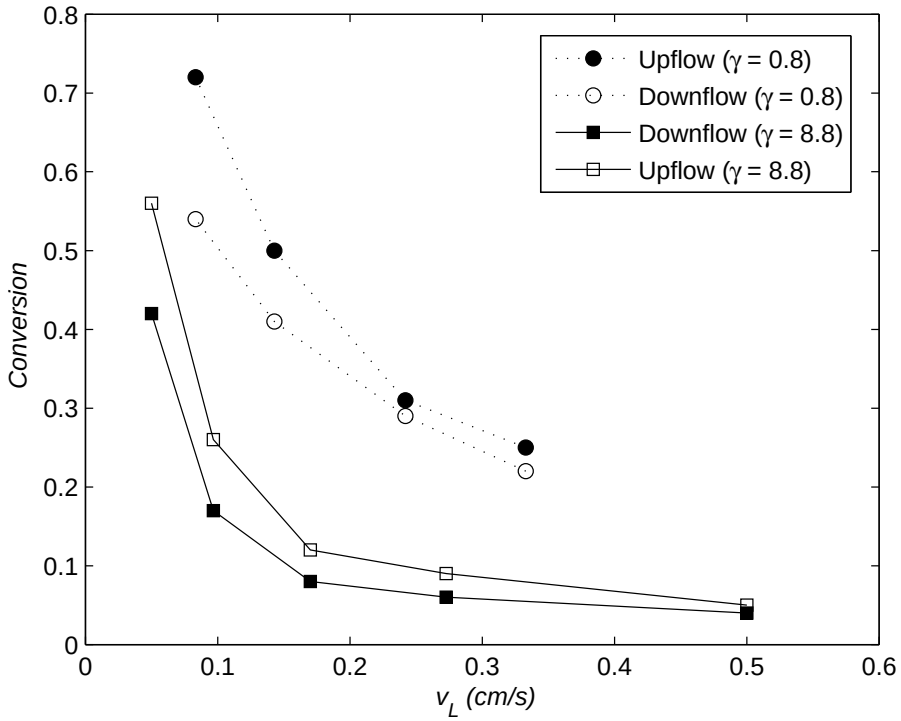

Figure 2.9: Upflow vs. downflow reactor performance for α-methylstyrene hydrogenation (Khadilkar et al., 1996)

2.3 Hydrogenation Kinetics

Accurate modelling and scale-up of industrially important reactions are made difficult by the complex hydrodynamic and mass transfer charactaristics of reactors, as well as reaction kinetics (Battsengel et al., 2002: 621). Kinetic models proposed by various authors for a specific reaction system differ due to different simplifying assumptions. These assumptions include the type of hydrogenation mechanisms, the rate determining step (RDS) as well as quasi-equilibrium hypothesis (Sarkar et al., 2006: 1149 - 1150).

2.3.1 Hydrogenation Mechanism

The type of hydrogenation mechanism is dependent on how adsorption of different species take place. The mechanism mostly accepted for heterogeneous noble-metal-catalyzed olefin hydrogenations is the Horiuti-Polanyi (HP) reaction sequence mechanism. According to the classic HP mechanism, chemical adsorption of the olefin takes place via chemisorption in a di-σ-adsorbed form on an active site (Horiuti & Polanyi, 1934: 1164). Spectroscopic and theoretical studies by Augustine et al. (1983: 1869) have shown that the π-adsorbed form of olefins on a single active site are the primary adsorption species during hydrogenations on $Pd/\gamma\text{-}Al_2O_3$ catalysts.

Cleavage of the double bond then takes place, accompanied by competitive dissociative adsorption of hydrogen. The hydrogen addition to the monohydrogenated complex and the desorption of the dihydrogenated complex are the only two irreversible steps in the mechanism, while the rest of the reversible steps account for double bond isomerization (Sarkar et al., 2006: 1149).

Langmuir-Hinshelwood kinetics is the term often used to describe single- and dual-site mechanisms. Single site π-adsorption of an olefin double bond occurs during hydrogenation reactions, while dissociative adsorption of hydrogen comprises of dual-site σ-adsorption of atomic hydrogen. The HP reaction sequence is shown in table 2.2.

Step 2 in table 2.2 (dissociative adsorption of H_2) can be altered to accommodate associative (single-site) adsorption by performing a simple site balance (equation 2.6). Kinetic models can now be developed by choosing a RDS before doing an overall active site balance on the catalyst surface.

$$H_2 + S \underset{k_{-H_2}}{\overset{k_{H_2}}{\leftrightarrows}} H_2S \tag{2.6}$$

Hydrogenation reactions can also follow the Eiley-Rideal mechanism or be classified as having non-competitive adsorption of dissociated/molecular hydrogen and alkenes (Meille et al., 2002: 1711). The non-competitive adsorption approach is discussed briefly in the next section. The Eiley-Rideal mechanism is a reaction between an adsorbed

Table 2.2: Horiuti-Polanyi reaction sequence for alkene hydrogenation

Step	Reaction	Rate
1	$A + S \underset{k_{-A}}{\overset{k_A}{\rightleftarrows}} AS$	$k_A C_A \theta_S - k_{-A}\theta_{AS}$
2	$H_2 + 2S \underset{k_{-H}}{\overset{k_H}{\rightleftarrows}} 2HS$	$k_H C_{H_2}\theta_S^2 - k_H \theta_{HS}$
3	$AS + HS \underset{k_{b1}}{\overset{k_{f1}}{\rightleftarrows}} AHS + S$	$k_{f1}\theta_{AS}\theta_{HS} - k_{b1}\theta_{AHS}\theta_S$
4	$AHS + HS \overset{k_{f2}}{\rightarrow} AH_2S + S$	$k_{f2}\theta_{AHS}\theta_{HS} - k_{b2}\theta_{AH_2S}\theta_S$
5	$AH_2S \underset{Fast}{\overset{k_{f3}}{\rightarrow}} AH_2 + S$	$k_{f3}\theta_{AH_2S}$

A - alkene; S - active site on catalyst surface; AH - monohydrogenated intermediate; AH_2 - hydrogenated product

molecule and a molecule in the gas phase (Fogler, 2006: 668), therefore no active sites are occupied by hydrogen during hydrogenation reactions while a partially dry surface is required for gas to make contact.

2.3.2 Rate Determining Step

The RDS of a chemical reaction is analogous to the neck of a funnel; the maximum rate at which liquid can flow through the funnel (maximum reaction rate) is limited by the width of the funnel neck (reaction rate of the RDS). Aspects to be considered in choosing a RDS in the absence of external mass transfer limitations include adsorption strength of reagents, internal diffusion, isomerization and hydroisomerization of the alkene. Weak adsorbtion of hydrogen will result in step two (table 2.2) to be rate-limiting as found by Holah et al. (1979: 148), who used a partially hydrogenated nickel boride catalyst.

In the HP sequence, isomerization of alkenes are assumed to take place only via the common monohydrogenated intermediate AHS (hydroisomerization). Experiments performed by Sarkar et al. (2006: 1149 - 1150) with 2 isooctene isomers in a nitrogen environment confirmed this assumption because no isomer traces were detected in the absence of hydrogen. These experiments also confirmed that olefin hydrogenation proceeds via a mechanism involving the single π-absorbed alkene species on a Pd/Al_2O_3 substrate as expected.

This is an important aspect to consider when choosing a RDS because the formation of the monohydrogenated intermediate differs completely for different isomers.

Canning et al. (2006: 27) found that the rate of 1-pentene and trans-2-pentene hydrogenation increased in the presence of competing isomers, while cis-2-pentene undergoes a reduction in reaction rate. If a mixture of isomers is present initially, reaction steps 1 and 3 in table 2.2 are duplicated for each isomer in order to compensate for competitive adsorption between isomers. Each duplicated step of reaction 3 should be considered as an RDS accordingly if the formation of the monohydrogenated intermediate is chosen as the RDS (Sarkar et al., 2006: 1150).

Most researchers have combined reaction step 5 with step 4 in table 2.2 to yield equation 2.7 below as an RDS (Uchytil et al., 1979: 147) and $\theta_{AH_2S} = 0$. Step 5 is regarded as extremely fast making it a good simplification. If the second H-addition is rate determining and step 3 is regarded as instantaneous, steps 3, 4 and 5 can be combined to yield equation 2.8.

$$AHS + HS \xrightarrow{k_{2+3}} AH_2 + 2S \tag{2.7}$$

$$AS + 2HS \xrightarrow{k_{1+2+3}} AH_2 + 3S \tag{2.8}$$

Some possible RDS's which can be identified from the classic HP reaction scheme are:

- Addition of first hydrogen (step 3 in table 2.2)
- Addition of second hydrogen to monohydrogenated intermediate (step 4 in table 2.2, equations 2.7 or 2.8)
- Single/dual site adsorption of hydrogen or alkene (competitive or non-competitive) for each alkene isomer (if present)

2.3.3 Quasi-equilibrium Hypothesis and Model Development

During a quasi-equilibrium (quasistatic) process, a system reaches equilibrium much faster, almost instantaneously, than its physical parameters vary (Fogler, 2006: 379). A quasistatic process is not necessarily reversible. Usually adsorption steps are assumed to be fast enough for the quasi-equilibrium hypothesis to be applied. The nett rate of reaction of such a step is equal to zero, which simplifies the rate expressions of steps 1 and 2 in table 2.2 to equations 2.9 and 2.10 for π-adsorbed alkene and dissociative adsorption of hydrogen respectively.

$$\theta_{AS} = K_A C_A \theta_S \tag{2.9}$$

$$\theta_{HS} = \sqrt{K_H C_{H_2}}\theta_S \tag{2.10}$$

Once again, the choice of reaction step to which the quasistatic hypothesis is applied will determine the form of the kinetic model obtained. The models in the following subsections are of the Langmuir-Hinshelwood-Hougen-Watson (LHHW) form with adsorption, surface and desorption reactions. These reactions are all expressed with power law expressions proportional to the fractional active surface coverage of reactants. Developement of a kinetic model now starts with assuming a pseudo-steady-state for one of the components in the reaction scheme taking part in the chosen RDS.

Model I

Quasistatic, competitive and dissosiative adsorption of H_2 and single site π-adsorption of the alkene is assumed with the traditional HP mechanism for the first model. The RDS is taken as the addition of the first H (step 3 in table 2.2). An active site balance on the catalyst surface gives equation 2.11:

$$\theta_{HS} + \theta_{AS} + \theta_{AHS} + \theta_{AH_2S} + \theta_S = 1 \tag{2.11}$$

Step 5 in table 2.2 is assumed to be radiply irreversible resulting in $\theta_{AH_2S} = 0$. Pseudostaticity assumption is now applied to the monohydrogenated intermediate AH (equation 2.12):

$$k_{f1}\theta_{AS}\theta_{HS} = k_{b1}\theta_{AHS}\theta_S + k_{f2+3}\theta_{AHS}\theta_{HS} \tag{2.12}$$

The vacant site fraction can be solved using equations 2.9, 2.10, 2.11 and 2.12 leading to equation 2.13. The rate of reaction for the alkene can be given as the rate of step 3 in the HP sequence, which results in the kinetic model in equation 2.14.

$$\theta_S = \frac{1}{1 + K_A C_A + \sqrt{K_H C_{H_2}} + \alpha}; \text{ where } \alpha = \frac{k_{f1} K_A C_A \sqrt{K_H C_{H_2}}}{k_{b1} + k_{f2+3}\sqrt{K_H C_{H_2}}} \tag{2.13}$$

$$r_{AH_2} = \frac{k_{f1} K_A C_A \sqrt{K_H C_{H_2}} - k_{b1}\alpha}{(1 + K_A C_A + \sqrt{K_H C_{H_2}} + \alpha)^2} \tag{2.14}$$

If the first H addition is considered irreversible and a lot slower than the addition of the second H, this model is simplified to equation 2.15 to yield less unknown system parameters. Similar models have been used previously for α-methylstyrene (Meille et al., 2002: 1712) and 1-butene (Bressa et al., 2003: 2088) hydrogenation.

$$r_{AH_2} = \frac{k_{f1} K_A C_A \sqrt{K_H C_{H_2}}}{(1 + K_A C_A + \sqrt{K_H C_{H_2}})^2} \tag{2.15}$$

Model II

If the rate determining step is the addition of the second H atom, equation 2.8 can be implemented into the mechanism, following the same procedure as in Model I to yield equation 2.16:

$$r_{AH_2} = \frac{k_{f1+2+3} K_A C_A K_H C_{H_2}}{(1 + K_A C_A + \sqrt{K_H C_{H_2}})^3} \tag{2.16}$$

This model has been utilized previously by Metaxas & Papayannakos (2006: 7112) for benzene hydrogenation, and kinetic parameters for this reaction have been determined by Roininen et al. (2009: 1868).

Models III and IV

For non-competitive adsorption of both species, $\theta_{S,A}$ and $\theta_{S,H}$ are the terms used to represent the vacant sites for alkene and hydrogen adsorption respectively. The active site balance is now performed for each adsorbed species separately (equations 2.17 and 2.18), as if two different types of sites are present for alkene and hydrogen adsorption respectively (Bressa et al., 2003: 2083).

$$\theta_{S,A} + \theta_{AS} = 1 \tag{2.17}$$

$$\theta_{S,H} + \theta_{HS} = 1 \tag{2.18}$$

For the two RDS's as in Model I and II, that is the formation of both the mono- and di-hydrogenated species, Models III and IV can be derived similarly and are shown by equations 2.19 and 2.20 respectively.

$$r_{AH_2} = \frac{k_{f1} K_A C_A \sqrt{K_H C_{H_2}}}{(1 + K_A C_A)(1 + \sqrt{K_H C_{H_2}})} \tag{2.19}$$

$$r_{AH_2} = \frac{k_{f1+2+3} K_A C_A K_H C_{H_2}}{(1 + K_A C_A)(1 + \sqrt{K_H C_{H_2}})^2} \tag{2.20}$$

Models V and VI

If molecular (associative) adsorption of hydrogen is assumed, the reaction in equation 2.21 will most likely occur because both H atoms get added simultaneously. The fractional

coverage of adsorbed hydrogen $\theta_{H_2S} = \theta_S K_{H_2} C_{H_2}$ can be derived by assuming pseudo-equilibrium for the reaction in equation 2.6, which is now used in the place of step 2 in the HP mechanism.

$$AS + H_2S \xrightarrow{k_{f4}} AH_2 + 2S \tag{2.21}$$

Following the same methodology and assumptions as with Models II and IV for competitive and non-competitive adsorption respectively, equations 2.22 and 2.23 can be derived:

$$r_{AH_2} = \frac{k_{f4} K_A C_A K_{H_2} C_{H_2}}{(1 + K_A C_A + K_{H_2} C_{H_2})^2} \tag{2.22}$$

$$r_{AH_2} = \frac{k_{f4} K_A C_A K_{H_2} C_{H_2}}{(1 + K_A C_A)(1 + K_{H_2} C_{H_2})} \tag{2.23}$$

2.3.4 Model Applications

Toppinen et al. (1997: 24) derived a model for alkylbenzene hydrogenation on a Ni/Al_2O_3 catalyst according to the classic HP reaction mechanism with competitive adsorption (equation 2.24). Their model was compatible for associative ($\gamma = 1$) and dissociative ($\gamma = 2$) adsorption of hydrogen. Equation 2.24 corresponds with models V and II from the previous section except for the coefficient of the $K_A C_A$ term which accounts for the three H_2 molecules that alkylbenzenes react with.

$$r_{AH_2} = \frac{k_{F1} K_A C_A K_{H_2} C_{H_2}}{(1 + 3K_A C_A + (K_{H_2} C_{H_2})^{1/\gamma})^{1+\gamma}} \tag{2.24}$$

Here k_{F1} denotes the rate constant for hydrogenating all three double bonds of the aromatic ring simultaneously. The fit of this kinetic model to experimental data with a heterogeneous reactor model was excellent, and kinetic parameters were determined for three different alkylbenzenes (Toppinen et al., 1997: 27).

Meille et al. (2002: 1714) assumed the RDS to be the addition of the second H, and non-competitive adsorption of α-methylstyrene and hydrogen as in model IV (equation 2.25). They reported similar activities with both low and high concentrations of α-methylstyrene and concluded a zeroth order dependency on its concentration in their kinetic expression. If α-methylstyrene adsorption is very strong and rapid, it can be shown that model IV reduces to equation 2.25.

$$r_{AH_2} = \frac{k_{f1+2+3} K_H C_{H_2}}{(1 + \sqrt{K_H C_{H_2}})^2} \tag{2.25}$$

Their model fit their experimental results excellently for 19 experiments with industrial size as well as for crushed catalyst particles. Battsengel et al. (2002: 6) accurately fitted a similar intrinsic rate equation to their experimental data for octene hydrogenation on supported nickel catalyst, and is shown by equation 2.26:

$$r_{AH_2} = \frac{k_1 C_A C_{H_2}}{(1 + k_2 C_{H_2})} = \frac{k_{f4} K_A C_A K_{H_2} C_{H_2}}{(1 + K_{H_2} C_{H_2})} \tag{2.26}$$

On close inspection of this rate equation one can notice that for very weak adsorption of the alkene and/or low alkene concentrations, model VI can be reduced to equation 2.26. Monteiro-Gezork et al. (2008: 474 - 482) did extensive Langmuir-Hinshelwood modelling with naphtalene hydrogenation in $NiMo-$, $Ni-$ and Ru/Al_2O_3 catalysts, with very good results. In the eight kinetic models they derived, models II, IV, V and VI from the previous section were also successfully fitted to their experimental work.

CHAPTER 3

EXPERIMENTAL

3.1 Reaction System Properties

The reaction of concern in this study is the heterogeneous hydrogenation of 1-octene. 1-Octene was supplied by Sasol with a purity of $> 99\%$, and a $C_{14} - C_{20}$ paraffin was used as solvent (Protea Chemicals). Ultra high purity H_2 and N_2 were used as the gas phase (Afrox). The liquid chemicals and their properties are shown in table 3.1.

Table 3.1: Properties of the reaction mixture liquid phase

Property	1-Octene	$C_{14} - C_{20}$ paraffin
Viscosity (mPa·s)	0.393	1.99
Density ($^{kg}/_{m^3}$)	714	770
Molar mass ($^{g}/_{mole}$)	112	230

A 0.3% ($^{w}/_{w}$) Pd/Al_2O_3 eggshell catalyst (Heraeus) was used to catalyze the hydrogenation of 1-octene. The catalyst is supplied in the form of 3 mm spherical particals with a density of 1100 $^{kg}/_{m^3}$ and a shell thickness of 0.3 mm. Some of the catalyst characteristics are shown in table 3.2 below.

Table 3.2: Catalyst features (Vannice & Singh, 2001: 1)

Property	Value
Volumetric fraction of active shell	0.49
Specific surface area of Palladium	0.55 $^{m^2}/_{g_{shell}}$
Tortuosity factor	1.5±0.6

3.2 Autoclave Reactor

3.2.1 Equipment

A Parr 4562 mini bench top reactor with a Parr 4843 controller was used for kinetic experiments (Parr Instrument Co.). A schematic diagram of the reactor setup is shown in figure 3.1.

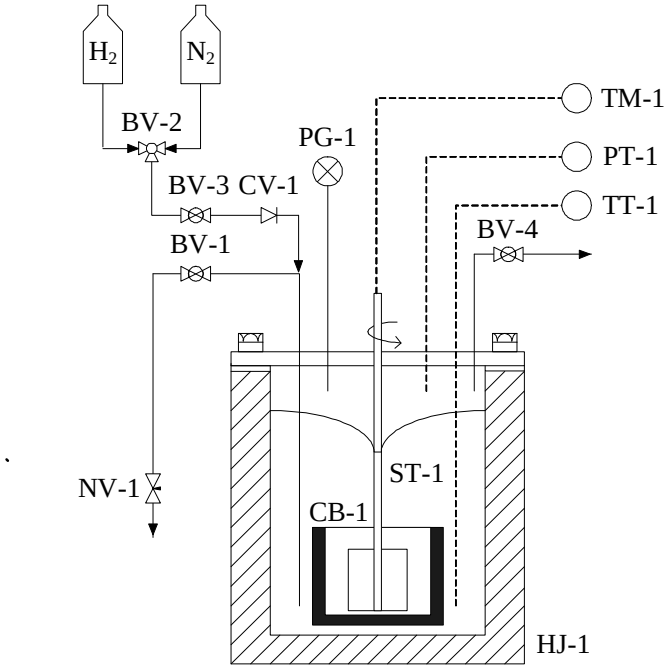

BV-1	Ball valve	NV-1	Needle valve
BV-2	Ball valve	PG-1	Pressure gauge
BV-3	Ball valve	PT-1	Pressure transmitter
BV-4	Ball valve	ST-1	Stirrer
CB-1	Catalyst basket	TM-1	Tachometer
HJ-1	Heating jacket	TT-1	Temperature transmitter

Figure 3.1: Autoclave reactor setup and instrumentation used for kinetic experiments

The autoclave or Robinson-Mahoney type reactor with a stationary catalytic basket (CB-1) consists of a cilyndrical vessel in which a baffled basket with an annular space neatly fits. The annular space holds the catalyst particles and consists of two cylindrical reinforced stainless steel sieves. The gas-entraining stirrer (ST-1) fits inside the basket while the thermocouple (TT-1) and gas inlet rests between the outside baffles. The stainless steel vessel has a volume of 450 ml, and is filled with liquid so that the gas-entrainment hole in the stirrer's hollow shaft remains above the liquid level. The stirrer speed and temperature is controlled by the Parr 4843 control box, while the pressure is manually regulated by a control valve on the feed line. Stainless steel pipes and Swagelok fittings were used on all lines, and six bolts and a teflon seal were used to connect the vessel to the reactor's head which is attached to the internals.

Because of the poor accuracy of the Parr reactor's transducer (10 psig), a 0-10 bar transducer was fitted on the head of the reactor with a 4-20 mA analogue output signal (PT-1). A NI USB6008 data aquisition box was used to record the data which is then imported into a spreadsheet. This addition increased the accuracy of the pressure recording to 1.2 kPa. An Agilent 6890N gas chromatographer was used to analyze samples to obtain octene conversion data.

3.2.2 Method

Gas-liquid mass transfer coefficient and Henry's law constant measurements

For gas-liquid mass transfer measurements a method was adopted from Pitault et al. (2005: 6251). They compared both gas-liquid and liquid-solid mass transfer in two types of catalytic basket reactors. The technique to measure $k_{GL}a$ involves the absorption of a soluble gas in an initially degassed liquid phase (Dietriech et al., 1992: 3598). This method holds various advantages, but the most important relevant to this study is that it allows one to measure the gas solubility in a particular reaction mixture.

The pressure transducer together with the data aquisition box recorded data at high speed without lag (20 hz). The gas phase and liquid phase for these experiments were H_2 gas and $C_{14} - C_{20}$ paraffin respectively, and the initial reaction mixture is degassed under known pressure P_0 and temperature T. Once stable equilibrium is reached, agitation is stopped and the system is pressurized to pressure P_m and is allowed to reach thermal equilibrium. Agitation is now started and the pressure drop due to gas absorption is recorded until a constant reactor pressure is again reached (P_f). Integrating a simple mass balance from $t = 0$ to t where $P(t) = P_f$, equations are obtained which can be fitted to the data in order to obtain $k_{GL}a$ and He (Pitault et al., 2005: 6251).

Once a pressure recording is made, a moving average function of 20 datapoints (1 second) was used on recorded data to smooth the curves. The He values obtained from these experiments were used in the modeling of the autoclave and packed bed reactors, and the $k_{GL}a$ values were used in modeling the gas-liquid mass transfer in the autoclave reactor. Various authors have reported He to be independant of pressure (Dietriech et al., 1992: 3), and He was assumed constant with the pressure variations during absorption runs in this work.

Kinetic experiments

A straightforward procedure was followed for the kinetic experiments. First a batch was created by mixing 1-octene with the paraffin. Because 100% conversion was obtained in each run, low initial 1-octene concentrations were used to limit the heat of reaction in order to run the reactor isothermally for an entire run (0.5% - 4% v/v). Pre-runs were

performed with the same batch of catalyst to verify stable catalytic activity. Catalyst activity decreased exponentially and stabilized after a few runs, and a pseudo first-order rate constant was fitted to experimental data for a number of runs. Catalyst was classified as stable when the variation of the rate constant between runs was $< 5\%$. Stable catalyst is packed into the catalytic basket, and voids are filled by homogeneously mixing inert 3 mm allumina spheres with the catalyst to completely fill the basket. The reason for this is to maintain the same hydrodynamic charactristics within the reactor for different amounts of active catalyst. Once the reactor is closed, agitation is started and the temperature is set to its setpoint.

Experimental runs were completed in the temperature range of 40 - 60 ℃, 4 - 36 bar pressure and 3 different stirrer speeds. At time $t = 0$, when the setpoint temperature is reached, the reactor is pressurized to the desired pressure. Isobaric operation was achieved because the gas reactant consumption rate was negligible relative to the amount of H_2 gas present in the gas phase once the liquid phase was saturated. Samples were taken initially and at 7 other time points and relative conversions were calculated from GC analysis. A sample is roughly 2 ml, and the total sampled volume for each run was limited to $< 5\%$ in order for the reaction to be modelled as a batch reaction.

Kinetic parameters were fitted by minimizing the average sum of absolute relative errors (AARE) between experimental and predicted conversions. The objective function is shown below in equation 3.1 for m experiments with n datapoints each.

$$AARE = \frac{1}{m}\sum_{j=1}^{m}\left(\sum_{i=1}^{n}\left(\frac{|x_{exp} - x_{pred}|}{x_{exp}}\right)_i\right)_j \tag{3.1}$$

3.3 Packed Bed Reactor

3.3.1 Equipment

The packed bed reactor used in this work was designed to operate in either co-current up- or downflow, or countercurrent flow of gas and liquid reagent. A schematic diagram of the experimental setup is shown in figure 3.2. A Bran & Luebbe H2-32 metering pump was used to pump the paraffin-octene mixture. From the pump the liquid is preheated to a temperature higher than the desired reactor temperature depending on the flow rate, before it enters the 1 m long 50 mm I.D column. The reactor was packed with 110 g (approximately 9 cm) of Pd/Al_2O_3 catalyst wedged in the middle of the bed between two 45.5 cm sections of 3 mm inert allumina support.

A distributor with a drip point density of 11000 m^2 is located at the top of the column, and liquid and gas are distributed from the bottom only by the catalyst retaining sieve plate (during upflow runs). Pressure is regulated with a back pressure regulator and gas flow is controlled by Brookes mass flow meters (0 - 30 $^{nL}/_{min}$). Eight internal

thermocouples are evenly distributed along the length of the reactor to verify isothermal operation, and heating jackets were used on the column for finer temperature control.

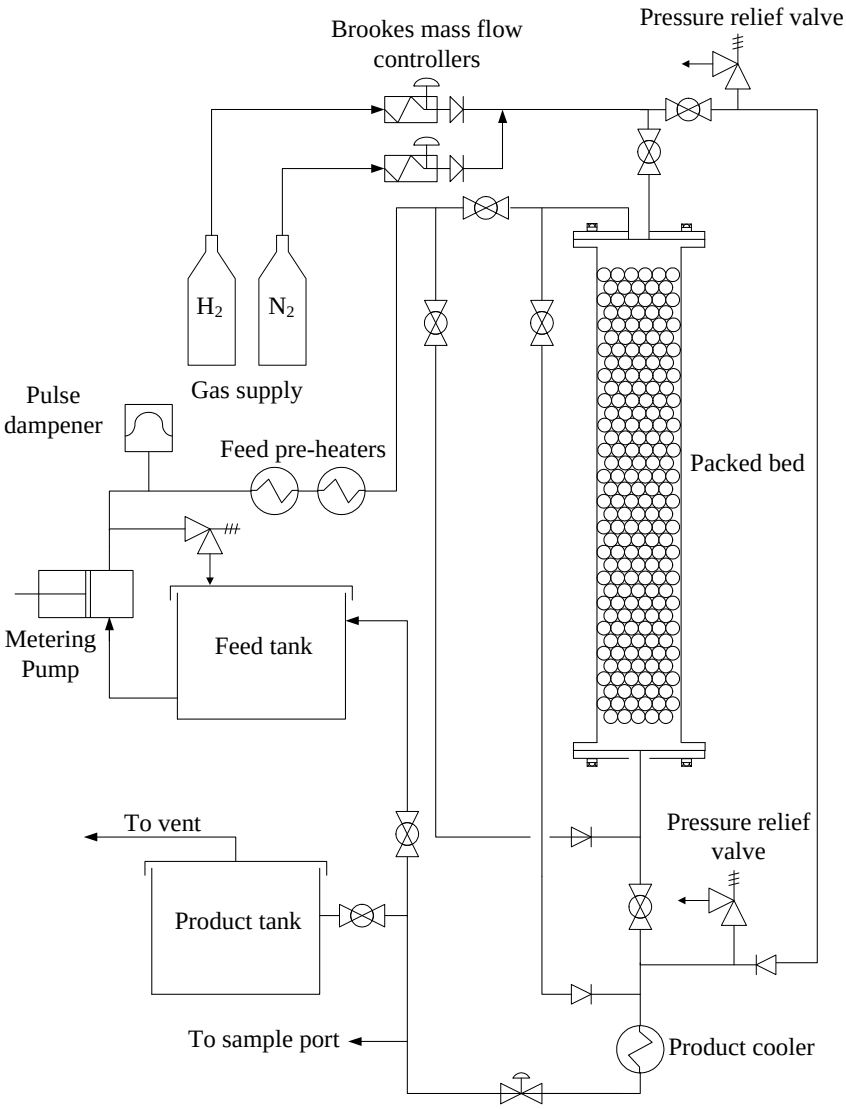

Figure 3.2: Schematic of the packed bed reactor setup

3.3.2 Method

Experiments were performed at gas limited conditions, that is high 1-octene concentrations and low partial pressure of H_2. Experimental runs were performed at 6 - 9 bar total pressure and 60 ℃, in 3 different operational modes: upflow, Levec-prewetted and extensively prewetted trickleflow. Inert allumina support was used with the catalyst to pack the column, and all runs were performed at 4 different liquid flow rates that correspond to superficial velocities of 1.70, 2.55, 3.40 and 5.09 $^{mm}/_{s}$. The metering pump was calibrated for 6 different stroke length and 10 stroke speeds, and the calibration curve is shown in figure 3.3. The same stroke lenght and speed was used to obtain the same flow

rate in every run to ensure better repeatability.

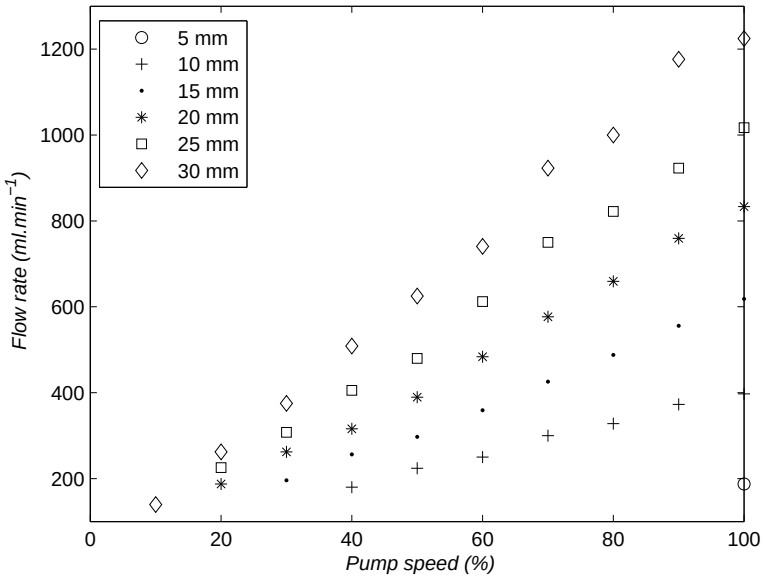

Figure 3.3: Pump calibration curves

The procedures for the three operational modes are as follows:

- *Upflow:* The pump stroke length and speed is set to obtain the desired flow rate, and the valves are manipulated so that the liquid enters at the bottom and exits at the top of the column. N_2 is introduced to simulate the total desired gas flow rate before the pre-heaters are set to their setpoint temperatures. Once steady state is reached, H_2 is introduced and the reaction starts. The flow through the system is on reflux to the feed tank until steady state which helps to completely mix the feed tank contents, and is switched to the product tank when hydrogen is first introduced.

- *Levec-prewetted trickle flow:* The bed is completely flooded, before valves are switched so that gas and liquid enters at the top and exits at the bottom of the column. The bottom of the reactor is opened and all liquid is allowed to freely drain. After no more liquid drips from the bottom, it is closed and the rest of the upflow start-up procedure is followed.

- *Extensively prewetted trickle flow:* The start-up procedure for this operational mode differes from Levec only by the fact that the bed is not drained, but co-current downflow of gas and liquid is commenced at operating flow rates after the bed is completely flooded.

For all experimental conditions, regime mappings were used to verify the interaction regime (Gianetto & Specchia, 1992: 3199). Using the criterion for dispersion by

Satterfield (1975: 224), dispersion effects can be neglected for conversions $< 95.2\%$. Gas-liquid mass transfer limitations were also investigated at experimental conditions where the slowest gas-liquid mass transfer were expected. This was done by comparing the reaction rates of the packed bed with that of the same bed where the active catalyst was homogeneously diluted throughout the entire length of the bed. If gas-liquid mass transfer has any rate limiting effect during a specific experimental run, higher reaction rates would be attained for that same run using a diluted catalytic bed. This is because less H_2 is then required per unit length of reactor, and the rate of depletion of H_2 with reactor length is slower in the diluted bed.

Two samples were taken about two residence times (based on voidage volume) apart at every set of experimental conditions to verify steady state. Wetting factors and liquid-solid mass transfer coefficients from a previous study (van Houwelingen, 2009: 80-85) were used in the modeling of the packed bed reactor, together with the determined kinetics from the autoclave reactor experiments.

CHAPTER 4

RESULTS AND DISCUSSION

4.1 Batch Reactor Kinetics

4.1.1 Gas-liquid Mass Transfer Coefficient and Hydrogen Solubility

To enable successful modeling of the autoclave reactor in order to fit kinetic parameters in the end, interphase mass transfer coefficients and gas saturation levels must be known. The method from Pitault et al. (2005) was adopted to measure gas-liquid mass transfer and hydrogen gas solubility. With this method a simple mass balance is performed over the liquid phase, and volumetric gas-liquid mass transfer coefficients ($k_{GL}a$) and Henry's law constants (He) are fitted to experimental pressure vs. time data. The resulting integrated equations are not derived here but are shown in equations 4.1 and 4.2. A typical pressure recording is shown in figure 4.1, with its respective linearized plot using equation 4.1. For four different stirrer speeds, the linear dimensionless pressure vs. time plots are shown in figure 4.2.

$$\frac{P_m - P_f}{P(t) - P_f} = exp\left(\frac{P_m - P_0}{P_f - P_0} k_{GL}a \cdot t\right) \tag{4.1}$$

$$\frac{P_f - P_0}{P_m - P_f} = He\frac{V_G}{V_L RT} \tag{4.2}$$

The slopes of these four linear lines are directly related to $k_{GL}a$ and can be evaluated. The Henry's law constant is evaluated using the initial and final pressures of the system, the temperature and different phase volumes. He was found to be independent of pressure in the experimental range of 3 - 6 bar, and was approximately 2.2 $^{mole}/_{m^3.bar}$ at 60℃. This value corresponds well to values found in the literature. For example, Florusse & Peters

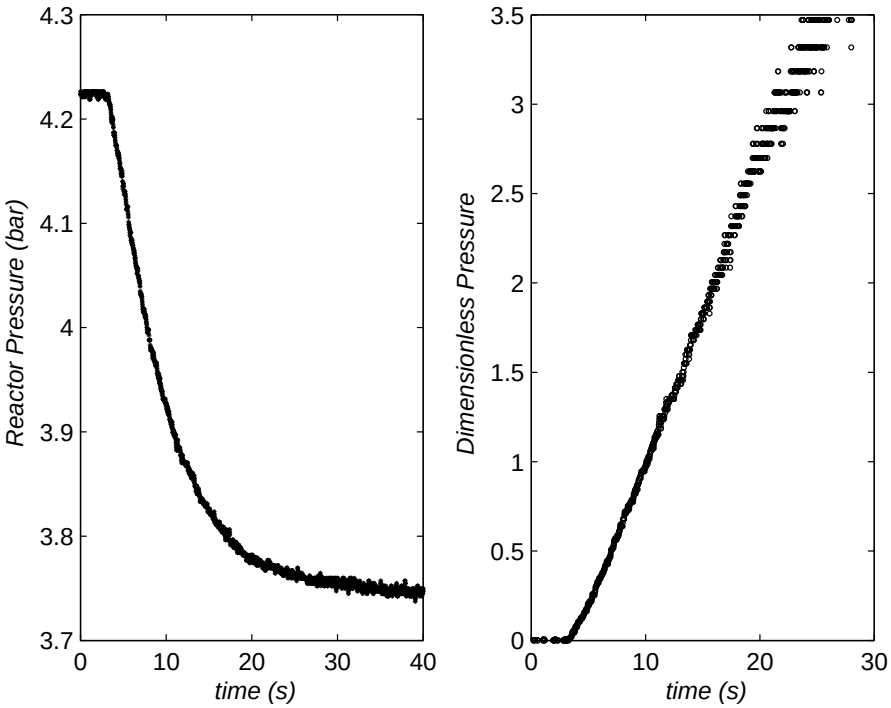

Figure 4.1: Typical pressure recording data and $k_{GL}a$ evaluation plot (1800 rpm)

(2003) found the solubility of hydrogen in hexadecane to be 3 $^{\text{mole}}/_{\text{m}^3.\text{bar}}$ at 60 ℃.

Catalyst basket packing charactaristics and liquid level inside the reactor exhibited interesting variations in $k_{GL}a$ measurements. All experimental work was done with a completely filled catalytic basket with similar liquid levels in each case to reproduce the same hydrodynamic behaviour for each run. The evaluated $k_{GL}a$ increased exponentially with stirrer speed, and the results show that $k_{GL}a \propto N^{5.3}$. The $k_{GL}a$ values as a function of stirrer speed is shown in figure 4.3, each stirrer speed with its respective confidence interval. The $k_{GL}a$ values increases a lot more rapidly than for the H_2/gas-oil system investigated by Pitault et al. (2005) who found $k_{GL}a \propto N^{3.4}$ for the exact same laboratory autoclave reactor. As noted on figure 4.3, $k_{GL}a$ rapidly increases at stirrer speeds greater than 1000 rpm. Pitault et al. (2005) also observed very slow gas-liquid mass transfer rates at stirrer speeds below 1000 rpm, where they measured very low gas holdup. From their experimental work, they found that the the gas holdup increased from 2% to 7% at stirrer speeds greater than 1000 rpm (critical stirrer speed).

The main advantage of this method to determine $k_{GL}a$ and He is that the same gas/liquid reagents and reaction system is used as for the succeeding kinetic experiments. This makes these parameters more applicable to the current system, and increases the accuracy of the modeling and fitted kinetic parameters.

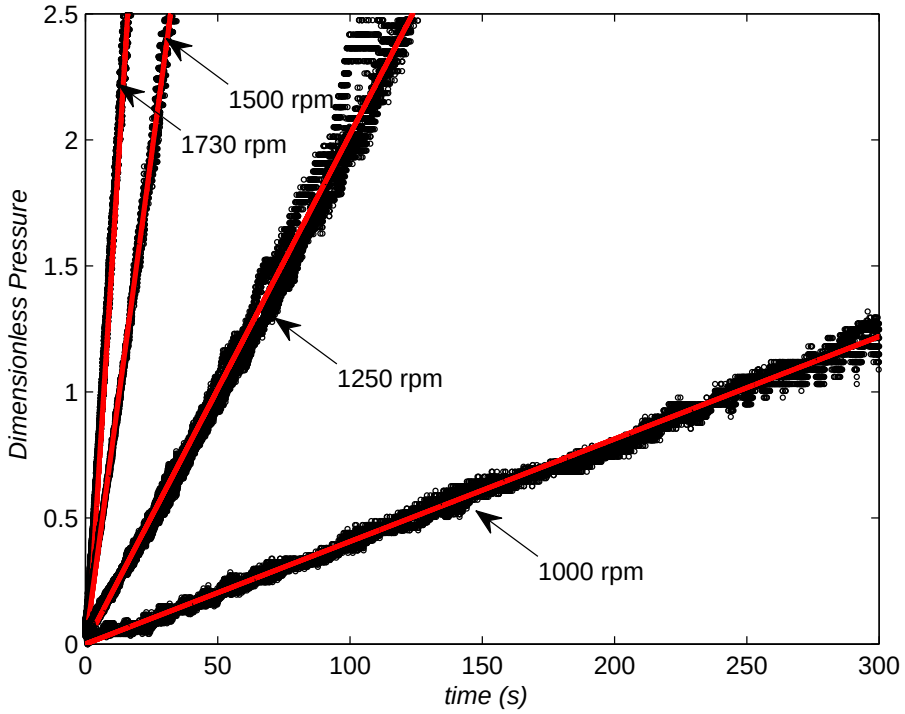

Figure 4.2: Dimensionless pressure (equation 4.1) variation with stirrer speed

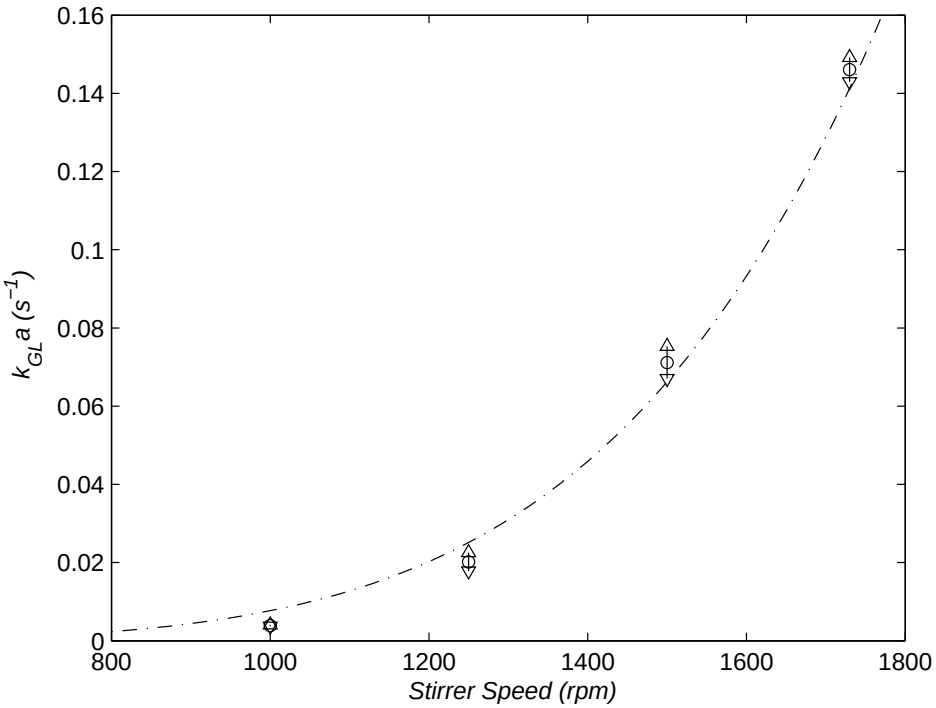

Figure 4.3: $k_{GL}a$ vs stirrer speed for the H_2/paraffin system

4.1.2 Catalyst Stability

Catalyst was found to reach stable activity after reacting to completion with a cumulative liquid reagent volume of about 2000 ml (2% octene v/v). Figure 4.4 shows how the fitted rate constants (at $p_{H_2} = 50$ bar and $T = 60$℃) decreased for the same batch of catalyst as a function of cumulative liquid reagent used.

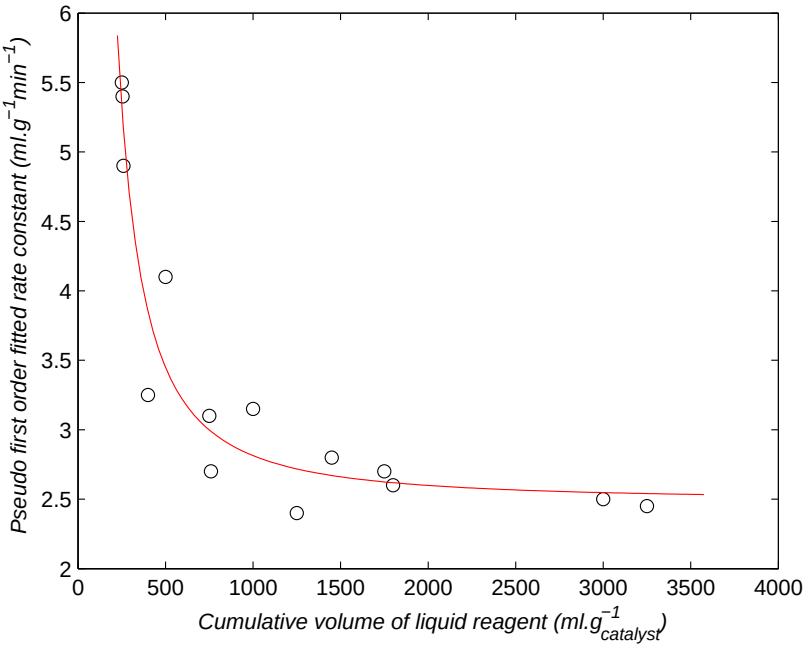

Figure 4.4: Stabilization of a batch of catalyst over a few repeated runs

4.1.3 Modeling and Liquid-Solid Mass Transfer Limitations

Langmuir-Hinshelwood rate kinetics were adopted for the modeling of the 1-octene hydrogenation. It was assumed that the particle kinetics obtained from batch autoclave experiments were adequate for the PBR analysis. The underlying assumption is that intra-particle hydrogen concentration gradients (if they exist) are similar for partially and fully wetted catalyst. This is a reasonable assumption considering that van Houwelingen et al. (2009) have shown that diffusional effects through the inactive center of the eggshell catalyst do not contribute significantly to the overall reaction. Liquid-solid mass transfer resistance steps were incorporated into the model for both reagents, and an additional gas-liquid resistance was included for the gas phase. The system equations used are listed below:

$$\frac{dC_{OCT,bulk}}{dt} = -r_{OCT} = f\left(C_{OCT,s}, C_{H_2,s}, k(T), K_{OCT}, K_H\right) \tag{4.3}$$

$$r_{OCT} = k_{LS}a_{LS}\left(C_{OCT,bulk} - C_{OCT,s}\right) = \beta k_{LS}a_{LS}\left(C_{H_2,bulk} - C_{H_2,s}\right) \tag{4.4}$$

$$\frac{dC_{H_2,bulk}}{dt} = k_{GL}a\left(p_{H_2}He - C_{H_2,bulk}\right) - \beta k_{LS}a_{LS}\left(C_{H_2,bulk} - C_{H_2,s}\right) \tag{4.5}$$

Because $k_{GL}a$ and He are known, the only unknowns are k_{LS}, β and the kinetic parameters. Mitrovic et al. (2005) measured liquid-solid mass transfer coefficients in a stationary catalytic basket reactor with similar dimensions as the one used in this work. In their study they also developed a correlation for k_{LS} which corrects for variations in fluid properties (equation 4.6).

$$Sh = \left(\frac{D_{octene}^{naphtol}}{D_{water}^{naphtol}}\right)^{0.66}\left(\frac{\rho_{octene}}{\rho_{water}}\frac{\mu_{water}}{\mu_{octene}}\right)^{0.47} \times 4.42 \times 10^{-3} Re_t^{0.8} Sc^{0.33} \tag{4.6}$$

Correlations were only used to obtain an initial estimation of k_{LS}. Once concentration profiles were obtained from integrating the system equations, liquid-solid mass transfer limitations could be visualized (if present) by plotting the surface to bulk concentration ratios (figure 4.5).

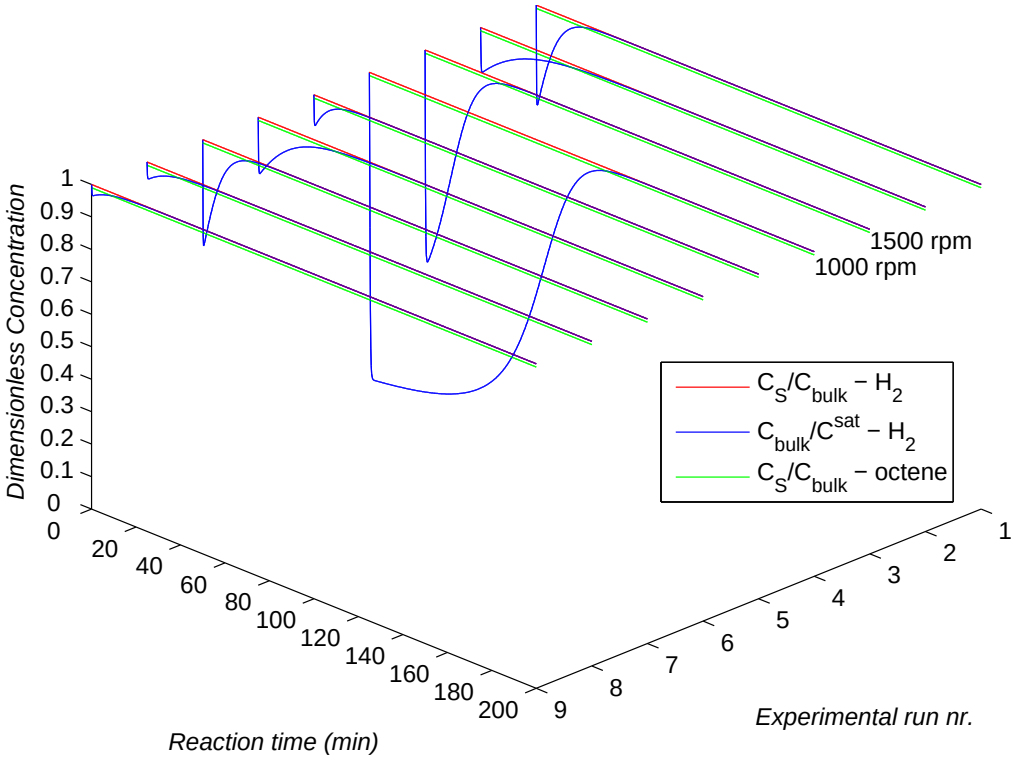

Figure 4.5: Surface:bulk concentration ratio plot to visualize liquid-solid mass transfer limitations. All runs at maximum stirrer speed except runs 3 and 4.

For the gas-reactant:liquid-reactant diffusivity ratio (β) within the solvent, a value of 4 was adopted from work on 1-octene hydrogenation studies by Battsengel et al. (2002) (Wilke-Chang correlation). The initial bulk H_2 concentrations were estimated as the saturated concentration, and initial surface concentrations were taken as the steady state values.

Concentration data profiles were obtained from kinetic experiments, and kinetic parameters were manipulated to obtain the best fit. Different kinetic models were evaluated, and the model with the best fit was used to interpret liquid-solid mass transfer effects. No liquid-solid mass transfer limitations were observed, and the plot of $\frac{C_{OCT,s}}{C_{OCT,bulk}}$ and $\frac{C_{H_2,s}}{C_{H_2,bulk}}$ remains unity for the entire duration of each experimental run (figure 4.5). Gas-liquid mass transfer limitations however can be observed at stirrer speeds of 1500 rpm and less, from the plot of $\frac{C_{H_2,bulk}}{C_{H_2}^{sat}}$. Because experimental values of $k_{GL}a$ and He were used in this model and liquid-solid mass transfer can be neglected (based on correlated values), the only remaining unknowns are the kinetic parameters.

4.1.4 Kinetic Model Evaluation and Fitted Parameters

For the 9 experimental runs shown in figure 4.5, experimental conditions are summarized in table 4.1. Six possible Langmuir-Hinshelwood kinetic models were fitted to the conversion data of each of these experiments. A single model is thus evaluated on its ability to predict reaction rates over a range of experimental conditions. The parity plot for each of the kinetic models are shown in figure 4.6, for the the parameters listed in table 4.2.

Table 4.1: Experimental conditions of kinetic experiments (excluding repeats)

Exp. run	W_{cat} (g)	p_{H_2} (bar)	T (°C)	$C_{OCT,0}$ ($^{mole}/_{L}$)	N (rpm)
1, 2	18, 6	4	40	0.13	1800
3, 4	18	4	40	0.13	1500, 1000
5	18	4	40	0.03	1800
6, 7	18, 6	4	60	0.13	1800
8, 9	18	20, 36	40	0.13	1800

Table 4.2: Fitted Langmuir-Hinshelwood kinetic parameters

Model	K_H($^{L}/_{mole}$)	K_{OCT}($^{L}/_{mole}$)	$k_{40°C}$ ($^{mole}/_{s.kg}$)	$k_{60°C}$ ($^{mole}/_{s.kg}$)	AARE %
I	0.12	0.24	7.0	8.2	4.9
II	16.10	0.23	4.4	5.2	4.8
II‡	2.19	0.12	1.0	1.5	-
III	1.02	0.13	4.4	5.1	4.8
IV	73.06	0.07	3.8	4.4	4.6
V	16.05	0.10	5.0	6.0	4.8
VI	57.96	0.03	4.8	5.7	4.6

‡Work by Toppinen et al. (1997) on toluene hydrogenation

Model IV and VI were the best fits each with a AARE of < 4.6 %. Model VI has however been used by previous researchers for octene hydrogenation on a supported nickel

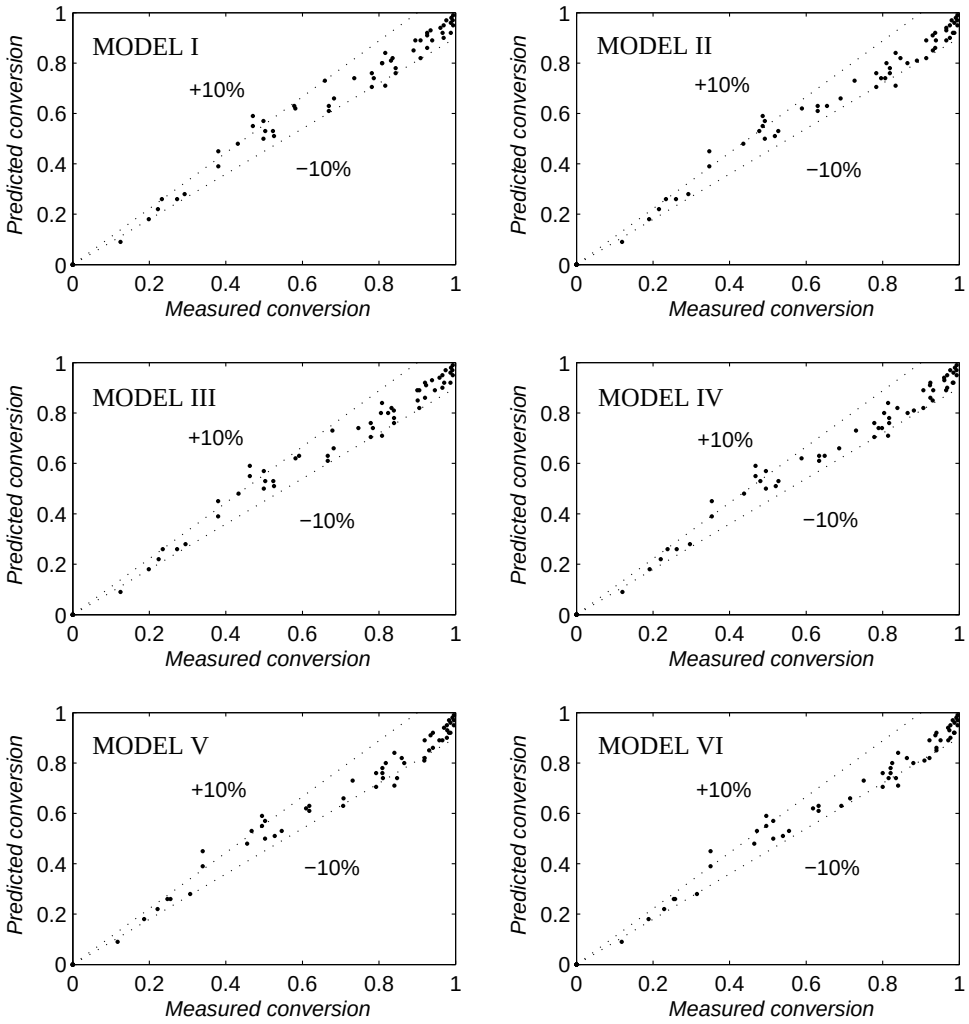

Figure 4.6: Parity plots for Langmuir-Hinshelwood kinetic models (I-VI)

catalyst (Battsengel et al., 2002: 6). They derived a kinetic model assuming dissociative and non-competitive adsorption of hydrogen and weak alkene adsoprtion onto active sites. The fitted adsorption constant for octene is three orders of magnitude smaller than that of hydrogen (table 4.2), which supports the weak alkene adsorption postulate. Model VI proved to be the least sensitive to initial value guesses and converged to an optimum global solution in the shortest computational time of all six models.

Considering the above, model VI is regarded as the most suitable to proceed with to model the packed bed reactor. Figure 4.7 shows the experimental and model predicted conversion data using model VI at the maximum stirrer speed, and 4.8 compares the reaction rates at the three different stirrer speeds.

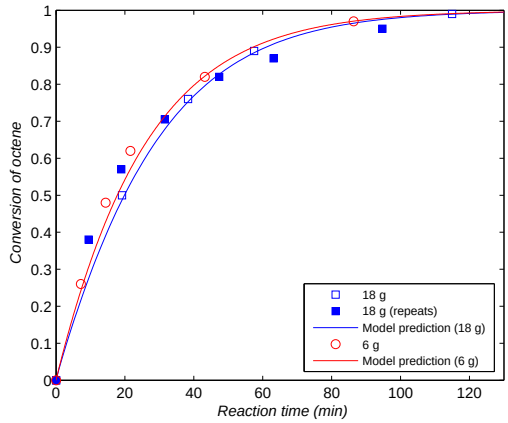

(a) 40℃, 4 bar, 1800 rpm

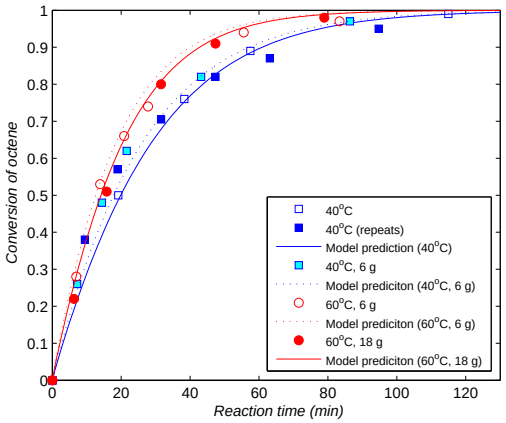

(b) 4 bar, 1800 rpm

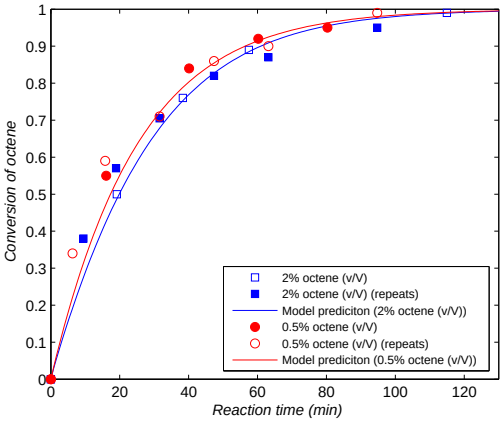

(c) 4 bar, 1800 rpm, 18 g, 40℃

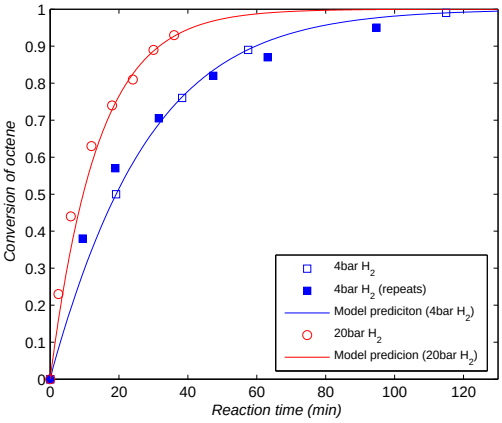

(d) 1800 rpm, 18 g, 40℃

Figure 4.7: Conversion data and model VI's prediction for all experimental runs (maximum stirrer speed)

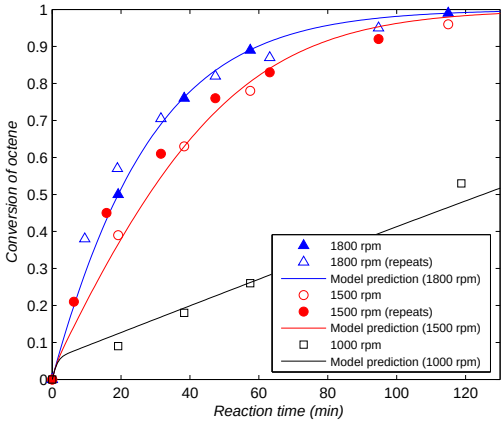

Figure 4.8: Conversion data and model VI's prediction for 3 stirrer speeds

4.2 Packed Bed Reactor Studies

Conventional knowledge on gas-limited reactions suggest that the dry catalyst area can have a rate enhancing effect. The effect has only been quantified by comparing upflow data (at assumably full wetting) to downflow data with partial wetting charactaristics. In the following section three different operational modes are compared: two downflow modes known to have different fractional wettings (van Houwelingen et al., 2006), as well as co-current upflow. Comparative reaction studies of three different operational modes with different wetting charactaristics allows one to quantify the contribution (if any) that dry catalyst areas exhibit.

4.2.1 Experimental Results

Five different sets of experimental conditions (table 4.3) were investigated for Levec prewetted, extensively prewetted as well as upflow modes. These 5 runs each consists of 3 dfferent operational modes, each with four different steady states corresponding to the four different liquid flow rates. The reported results thus consist of 60 steady state octene conversion values, reported as average reaction rates. The model predicted conversion profile was observed to be linear with reaction length in the experimental conversion range of below 44%. Considering this, the average reaction rates (overall conversion) were considered adequate to quantify reaction rates for comparison purposes. Experimental conditions of run 3 and 4 were chosen as such to enable one to investigate the effect of flow regime while keeping the extent of gas-limitation (γ) constant. Runs 1 and 4 had similar gas mass fluxes with different γ values to investigate the effect of the extent of gas reactant limitation within the same hydrodynamic regime, while run 3 consisted of a γ and gas mass flux roughly inbetween that of runs 1 and 4.

Run 5 was performed after run 4 where the catalyst bed section was homogeneously diluted with inert allumina spheres throughout the entire length of the bed. This was done in order to decrease the H_2 reactant demand (consumption rate) per unit length of bed, in order to quantify the rate limiting effect of gas-liquid mass transfer on the short bed section (runs 1 - 4). For instance if the diluted bed of run 4 gave rise to higher reaction rates, then one could conclude that gas-liquid mass transfer governs the overall reaction rate of run 4.

The liquid velocities were 200, 300, 400 and 600 $^{ml}/_{min}$, corresponding to superficial velocities of 1.7, 2.5, 3.4 and 5.1 $^{mm}/_{s}$ respectively. Two residence times were allowed between samples for steady state, based on voidage volume. These times corresponded to 8, 5, 4 and 3 minutes for the four liquid flow rates respectively. The overall reaction rates of the five experimental runs are shown in figure 4.9. To better vizualize the effect of different experimental conditions (γ and v_G) on the performance of each operational mode, figure 4.10 shows all the results for each mode individually.

Table 4.3: Packed bed reaction studies experimental conditions

Run nr.	1	2	3	4	5
γ-factor	60	30	15	15	15
v_G ($^{mm}/_{s}$)	16	16	16	16	16
M_G ($^{g}/_{mole}$)	24	19	11	16	16
P_{total} (bar)	6	6	6	9	9
p_{H_2} (bar)	0.9	2	4	4	4
ρ_G ($^{kg}/_{m^3}$)	5.2	4.2	2.3	5.4	5.4

4.2.2 Discussion

As seen from the results (figure 4.9), decreasing the gas density in run 1 from 5.2 $^{kg}/_{m^3}$ to 4.2 $^{kg}/_{m^3}$ (run 2), drastically increases the upflow performance. Downflow reaction rates also increased slightly with this gas density decrease, but not to the same extent as upflow. With a further increase in ρ_G from 4.2 $^{kg}/_{m^3}$ (run 2) to 2.3 $^{kg}/_{m^3}$ (run 3), the same trend continues. With this gas density decrease, the extent of gas limitation (γ) is also decreased. Increasing the gas density to that of run 1 with the same γ-value (run 4), upflow performance once again decreases to below that of downflow.

In every run (1 - 5) extensively prewetted trickle flow outperformed the Levec prewetted beds, despite the Levec bed having a lower wetting efficiency. It was also noted that the reaction rates of both modes (especially downflow) dropped drastically when run 4 was repeated with the diluted bed in run 5. Upflow reaction rates were expected to increase in run 5 because of the effective increase in $k_{GL}a$ in the reactive section of the bed. Very low reaction rates were observed in run 5, and the experimental results could not entirely confirm any performance switch. A possible inhibitant could have caused the unexpected results, and run 5 can accordingly only be used for trend comparison and not absolute reaction rates. Possible causes considered for the unexpected and decrease in reaction rates include:

- Inhibiting or catalyst poisoning effect of impurities present in the liquid phase because a different batch of 1-octene was used for run 5
- Presence of other alkenes favoured by selective hydrogenation (1% - 2% hexene)

For all 5 experimental runs extensively prewetted downflow exhibited higher reaction rates than Levec prewetted downflow at all liquid velocities despite having a higher wetting efficiency. The generally accepted assumption that dry area mass transfer contributes to increased reaction rates is thus not confirmed in this study.

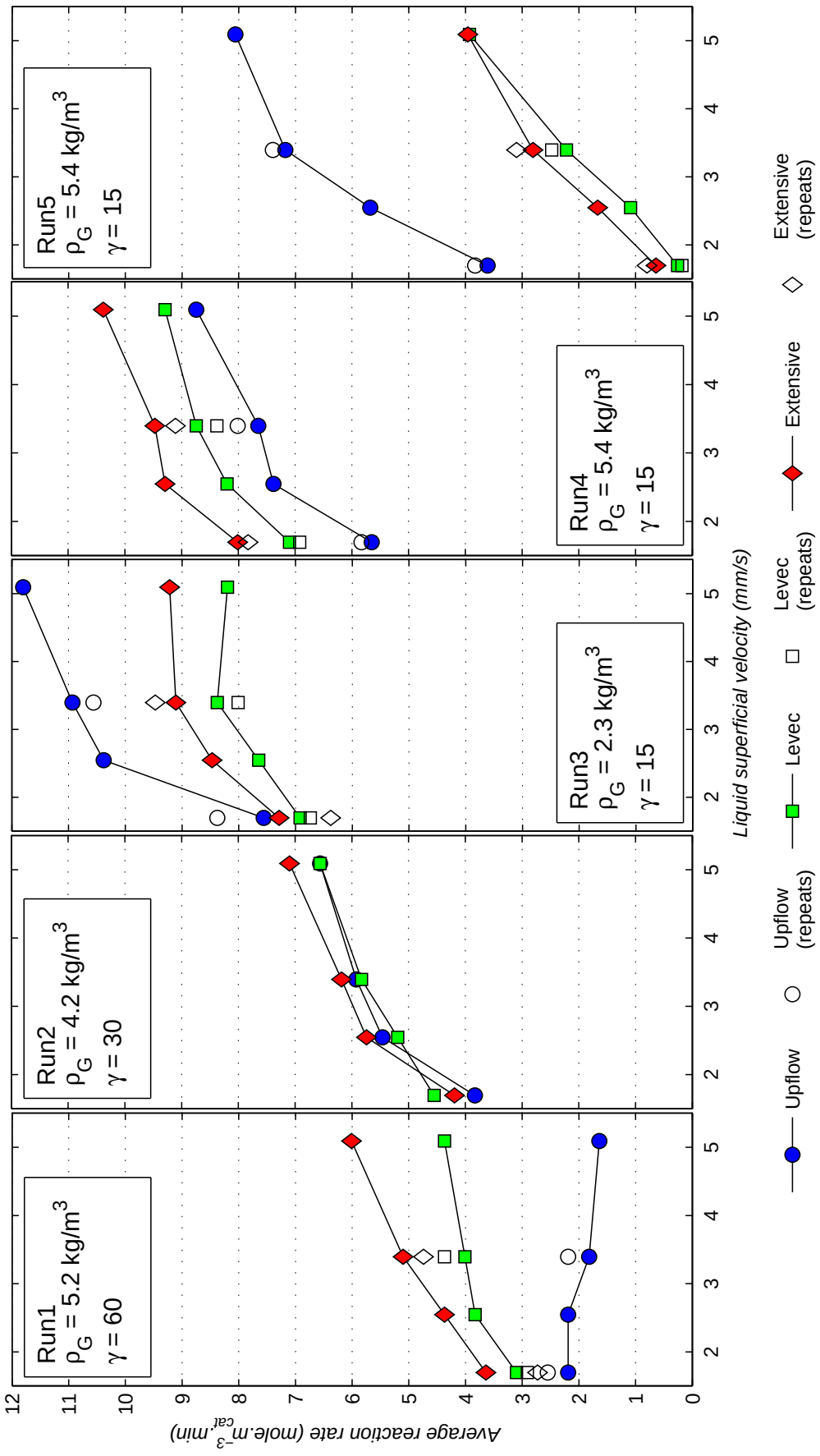

Figure 4.9: Experimental runs 1 - 5 (experimental conditions shown in table 4.3)

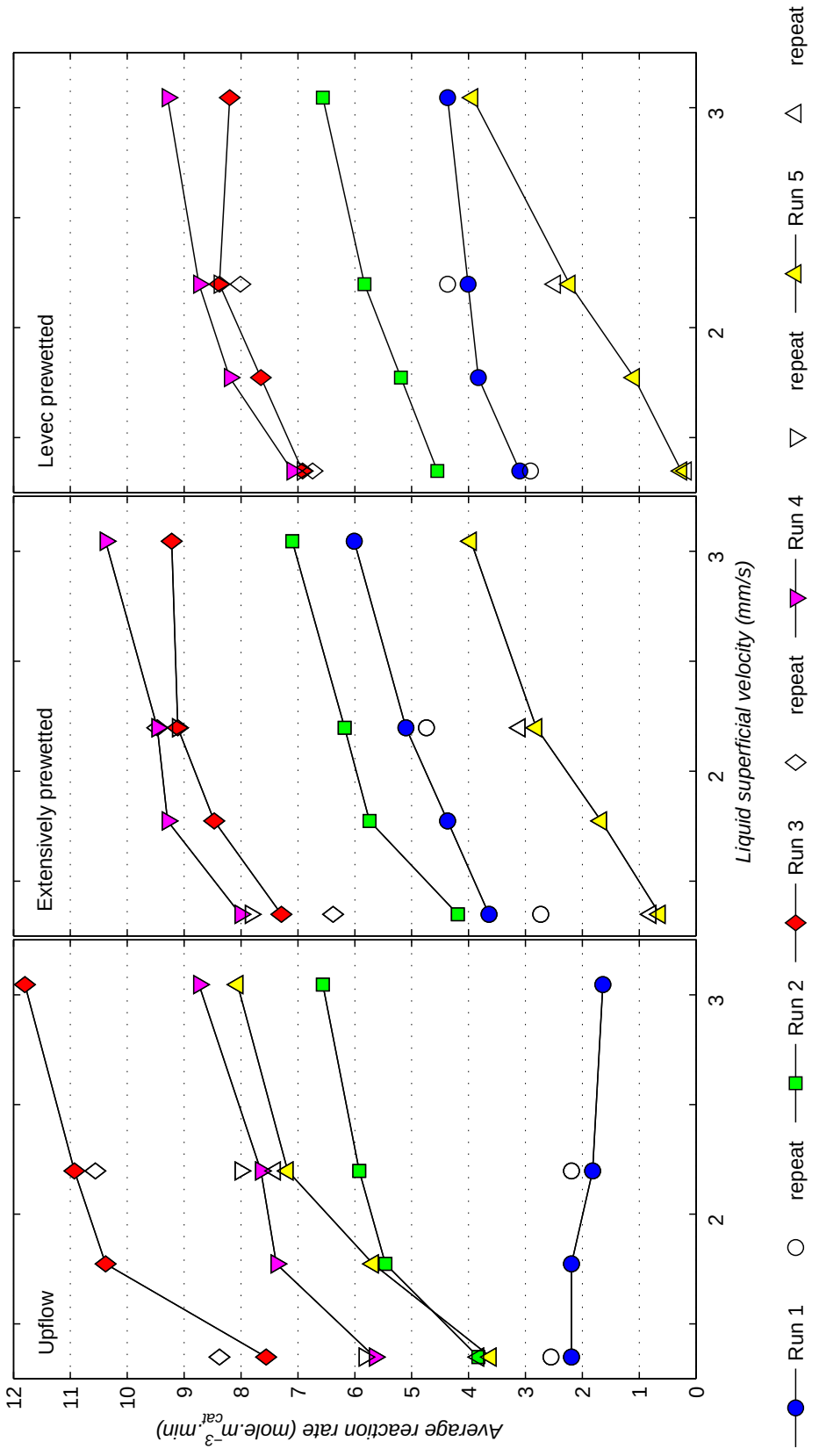

Figure 4.10: Experimental rate data for each operational mode, (Upflow - left, Levec - right)

Regarding operational mode, the results show that the conventional downflow/upflow argument for gas-limited conditions, that downflow is favoured due to lower wetting efficiency, could not be confirmed. Four experimental runs were performed, the only differences between these runs being the extent of gas limitation (γ) and gas density. Although experimental runs 1 and 4 had a smaller observed reaction rate for the upflow operation, the trend could not be confirmed by the downflow operation where the extensively prewetted bed outperformed the Levec-bed in all experimental runs.

The main reason for the rate differences lies in the difference between the external mass transfer steps, that is liquid side liquid-solid and gas-lquid mass transfer. Axial dispersion can be neglected due to the packing and column dimensions, considering the general criterion by Satterfield (1975) which states that axial dispersion is negligible when $\frac{l}{d_p} > \frac{20n}{Pe_L} ln \frac{C_{in}}{C_{out}}$, which was the case here even at the highest conversion (44 %). Extensively prewetted downflow is known to outperform Levec prewetted downflow in both gas-liquid (Loudon et al., 2006) and liquid-solid mass transfer (Joubert & Nicol, 2009). These differences dominate the outcome of the overall rate, also for the upflow operation where the external mass transfer steps are highly dependent on the hydrodynamic regime.

The fact that downflow outperformed upflow in runs 1 and 4 can thus rather be attributed to a possibility of slugging in the upflow mode because of their higher gas mass fluxes, instead of a dry area contribution effect. This work as well as some literature reported studies operated in a possible hybrid regime of slugging and bubbling (figure 4.11), while low interaction trickle flow was verified for all downflow experiments in this study.

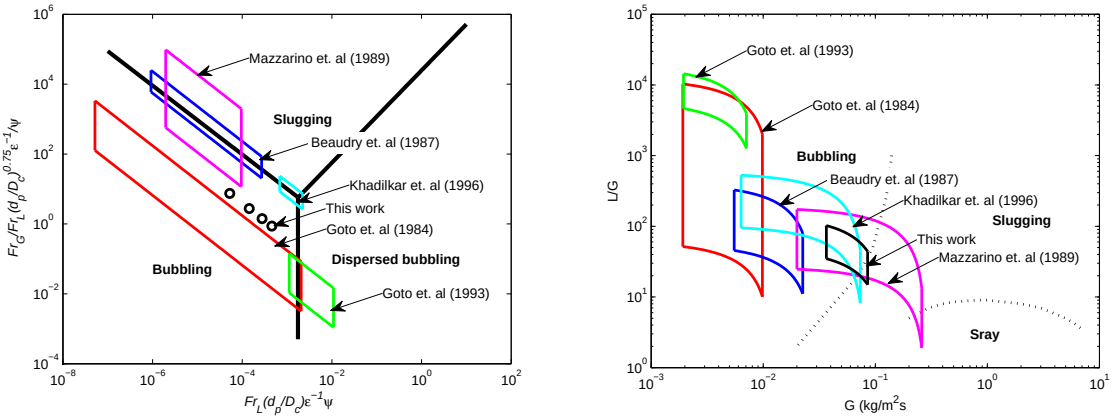

(a) Murugesan & Sivakumar (2002) (b) Gianetto & Specchia (1992)

Figure 4.11: Regime mappings by two different authors for packed bubble columns

From figure 4.11 it is evident that reactors from previous studies might have experienced slugging behaviour. Especially the gas-limited experiments from Beaudry et al. (1987) and Khadilkar et al. (1996) who studied α-methylstyrene hydrogenation, operated in the slug-flow regime according to the above regime mappings. Their liquid-limited re-

actions however operated in the bubbling regime. The fact that Khadilkar et al. (1996) (who developed the γ-criterion) operated in the slug flow regime during gas-limited experiments, makes the γ criterion subject to criticism. Because no dry area effects can be concluded from figure 4.9 and because upflow rates shift remarkably, hydrodynamic regime (slug vs bubbling) effects are the most likely cause. It is highly likely that the γ-pronouncements for up-/downflow from Khadilkar et al. (1996) can be explained by a possible regime shift effect instead of gas-solid direct mass transfer.

4.2.3 Modeling

The predetermined particle kinetics from the previous subsection together with experimental wetting-based liquid-solid mass transfer coefficients from the same reactor setup (van Houwelingen, 2009) was used to model the reaction (table 4.4). A similar three-phase model was used as for the autoclave reactor, with gas-solid mass transfer assumed negligible. The model equations are shown below:

$$\frac{dC_{OCT,bulk}}{dt} = -r_{OCT} \tag{4.7}$$

$$r_{OCT} = f_w k_{LS} a_{LS} \left(C_{OCT,bulk} - C_{OCT,s}\right) \tag{4.8}$$

$$r_{OCT} == \beta f_w k_{LS} a_{LS} \left(C_{H_2,bulk} - C_{H_2,s}\right) \tag{4.9}$$

$$\frac{dC_{H_2,bulk}}{dt} = k_{GL}a\left(\frac{p_{H_2}}{He} - C_{H_2,bulk}\right) - \beta f_w k_{LS} a_{LS} \left(C_{H_2,bulk} - C_{H_2,s}\right) \tag{4.10}$$

$$r_{OCT} = f\left(C_{OCT,s}, C_{H_2,s}, k(T), K_{OCT}, K_H\right) \tag{4.11}$$

Table 4.4: Liquid-solid mass transfer coefficients used in the model (van Houwelingen, 2009)

v_L (mm/s)	$f_w k_{LS,up}$ (m/s $\times 10^5$)	$f_w k_{LS,EXT}$ (m/s $\times 10^5$)	$f_w k_{LS,LEV}$ (m/s $\times 10^5$)
1.7	2.60	2.10	1.75
2.5	2.95	2.40	2.10
3.4	3.25	2.75	2.40
5.1	3.80	3.00	2.70

With no gas-liquid mass transfer step, predicted average conversions were much greater than experimental conversions. $k_{GL}a$ values were thus fitted in order to minimize the error of experimental and predicted average conversions. To illustrate the hydrodynamic model, the upflow mode of two different catalytic beds are compared. Because

slugging during upflow (runs 4 and 5) is thought to have detrimental effects on gas-liquid mass transfer and because experimental data from run 5 is discarded, the extent of this effect could be predicted by diluting the bed. This decreases the rate at which H_2 is consumed by the catalyst per length of bed, reducing the chances of gas reactant getting depleted along the bed.

To visualize this effect consider the simulated concentration profiles of runs 4 and 5 (figure 4.12). For the short section of catalyst bed (9 cm) the bulk liquid and catalyst surface concentrations drops drastically at the beginning of the bed and gets depleted. The reaction rate is now controlled by the rate of external gas-liquid mass transfer rate. For the diluted bed (1 m) the concentration drops and increases to the saturation level along the length of the bed. The effect of gas-liquid mass transfer limitation is thus decreased and much higher reaction rates are predicted.

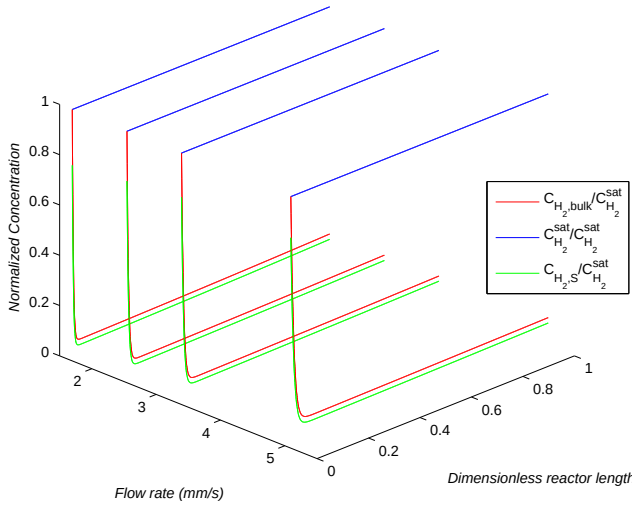

(a) Run 4

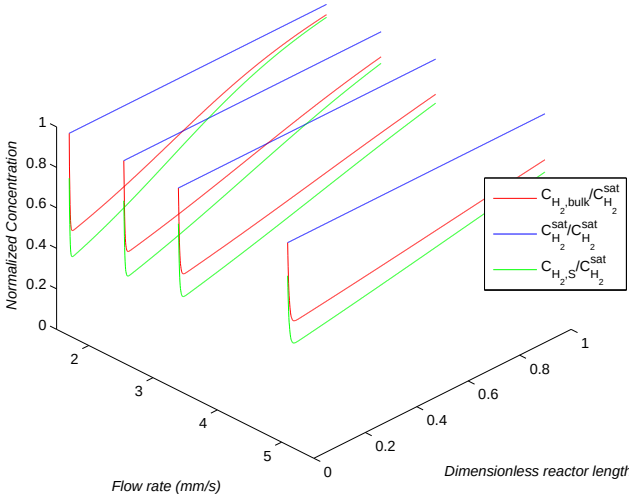

(b) Run 5 (diluted bed)

Figure 4.12: Concentration profiles for the 9 cm (run 4) section and 1 m (run 5) homogeneously diluted catalyst beds (both upflow mode)

A sensitivity analysis of $f_w k_{LS}$ was performed on runs 1 - 4, and model predictions were not noticeably affected by any increase in $f_w k_{LS}$. Only once $f_w k_{LS}$ values were multiplied by a factor of 0.5 or less, were reaction rate predictions observed to be markedly affected by the alterations. The same was observed during a sensitivity test on the proportional kinetic rate constant $k(T)$. It can thus be concluded that the overall reaction rate is limited by the rate of gas-liquid mass transfer.

The complete absence of liquid-solid mass transfer limitations were however not verified by the model, and figure 4.13 shows the average ratios of surface:bulk hydrogen concentration for runs 1 - 4 (extensively prewetted). According to the figure, calculated average surface:bulk H_2 concentration ratios varied between 70% and 85%. Considering this, liquid-solid mass transfer still affects reactions but to a much lesser extent than gas-liquid mass transfer which is regarded as the overall rate governing transport step.

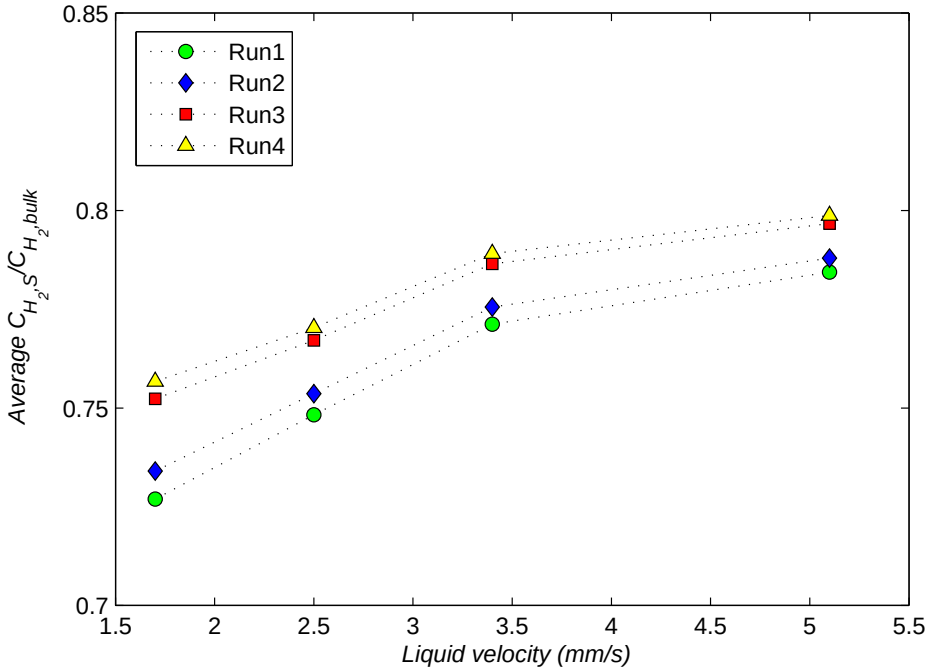

Figure 4.13: Average H_2 surface:bulk values of the concentration profiles through the length of the bed (runs 1 - 4)

The fitted $k_{GL}a$ values for runs 1 - 4 are shown in figure 4.14. As seen from the figure, the $k_{GL}a$ trend for upflow is not consistent with that of the two downflow runs. According to the regime mappings in figure 4.11 and experimental results, runs 1, 4 and 5 (higher gas mass fluxes) operate in a regime with a certain degree of slugging in the upflow mode. This could be a plausible explanation for the observed variation in fitted $k_{GL}a$ values during upflow. One would expect a lot smaller variation in $k_{GL}a$ between upflow/downflow experimental runs. Conventionally gas-liquid mass transfer is not believed to be such a strong function of gas density as observed in this study.

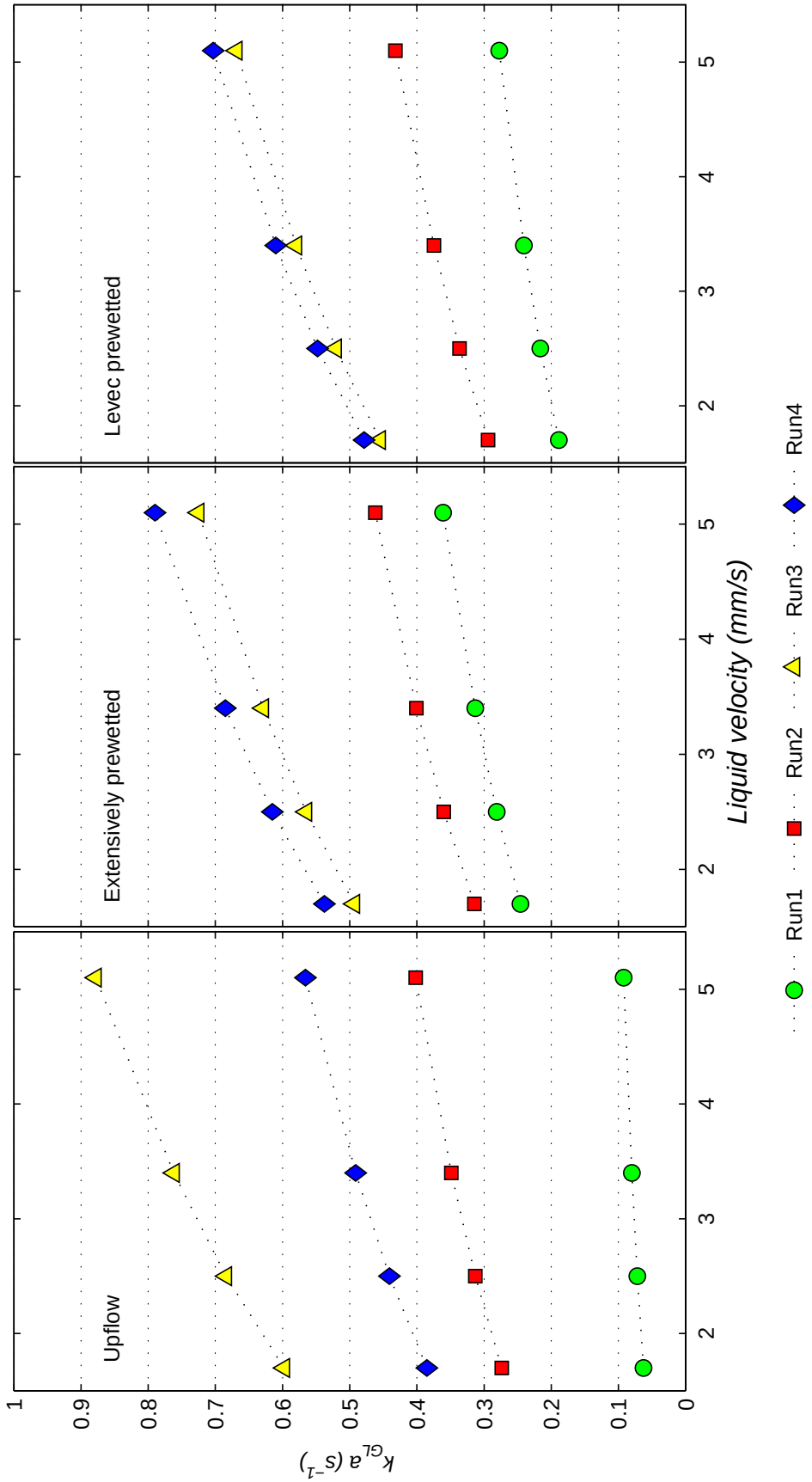

Figure 4.14: Fitted $k_{GL}a$ values for runs 1 - 5 (Upflow - left, Levec - right)

The total relative error for the fitted $k_{GL}a$ values to predict experimental conversions were 11% for upflow and less than 5% for the two downflow modes (runs 1 - 4). A general correlation was fitted to runs 1 - 4 for all three operational modes to get a monotonic $k_{GL}a$ value as a function of liquid velocity. The correlation was of the form $k_{GL}a = K \times v_L^{0.35}$, with $K = 0.6 - 5.6$ for upflow and $K = 2.3 - 5.0$ for downflow respectively. The proportional constant K was noted to be proportional to the total system pressure and inversely proportional the average gas molar mass M_G. No definite trend was noticed for the fitted $k_{GL}a$ values in the upflow mode.

Neglecting run 5, the correlation for downflow becomes $k_{GL}a \approx \frac{aP_{tot}}{M_G} v_L^{0.35}$ with P_{tot} in bar and M_G in $^{g}/_{mole}$. The value of a is roughly 7.7 and 8.8 for Levec and extensively prewetted downflow beds respectively. This correlation predicted the fitted $k_{GL}a$ values to within 5% (figure 4.15).

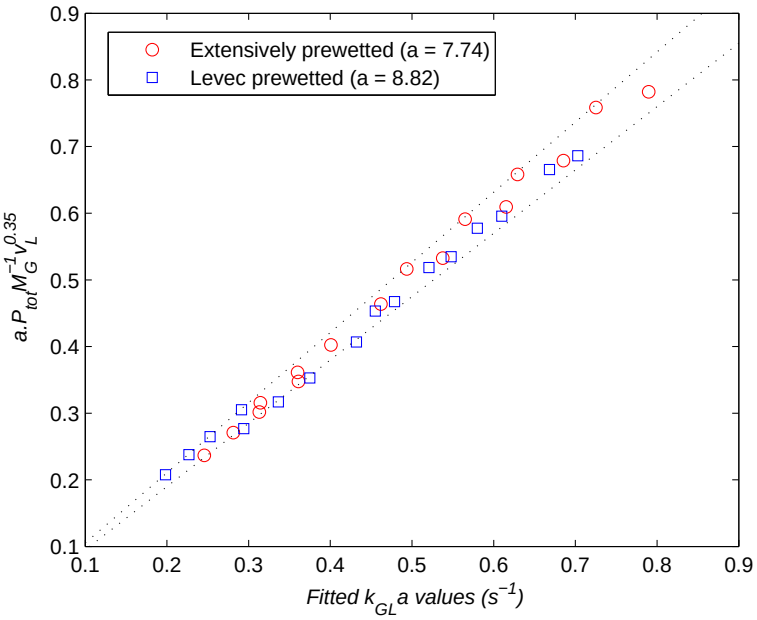

Figure 4.15: $k_{GL}a$ correlation vs. fitted values parity plot

It has been shown previously that beyond certain critical gas velocities (approximately 20 $^{mm}/_{s}$), the trickle flow regime becomes gas inertia dominated (Larachi et al., 1992). Because the gas viscosity is insensitive to pressure, the gas-liquid interfacial area is not influenced by gas density via pressure. Because interfacial gas-liquid area decreases with gas density (Larachi et al., 1992), higher gas molar mass would result in such a decrease. This coincides well with the experimental findings in this work.

Because the gas-side gas-liquid mass transfer coefficient is expected to diminish with high pressure operation (Dudukovic et al., 1999), and because experimental work in this study commenced at moderate to low pressures, k_Ga may not be ignored. Regarding the total pressure, if the gas-side gas-liquid mass transfer coefficient is not negligible, the

driving force for overall gas-liquid mass transfer becomes dependent on the total system pressure. It can be shown that the overall gas-liquid mass transfer depends on both the gas and liquid side:

$$\frac{1}{k_{GL}a} = \frac{1}{k_G a} + \frac{m}{k_L a} \tag{4.12}$$

In equation 4.12, m is given by $\frac{He.\rho_L}{P_{tot}}$ when $p_A = He.C_A^*$. Inspection of equation 4.12 reveals that an increase of total pressure will result in an increase of the overall gas-liquid mass transfer coefficient. It thus becomes clear that a balance between gas-side driving force via total pressure, and momentum and shear variations at the interface influenced by gas molar mass and viscosity exists. No similar correlations were obtained in the literature to predict $k_{GL}a$, and so no definite conclusions can be drawn regarding the effect of gas properties on the observed gas-liquid mass transfer variations.

CHAPTER 5

CONCLUSIONS

Gas-liquid mass transfer, hydrogen solubility and particle rate kinetics were measured in a 450 ml laboratory autoclave reactor fitted with a gas entrainment stirrer. $Pd\text{-}Al_2O_3$ eggshell (0.3% $^{w}/_{w}$) spheres were used to catalyze the 1-octene hydrogenation reaction under gas limited conditions $\left(\gamma = \frac{D_{e,octene}C_{octene}}{D_{e,H_2}C_{H_2}} >> 1\right)$. Conclusions drawn from the autoclave reactor experimental work include:

- Gas-liquid mass transfer between H_2 and the paraffin increased exponentially above the critical stirrer speed of 1000 rpm according to the relation $k_{GL}a = 8.97 \times 10^{-19}N^{5.31}(s^{-1})$. This is because an increase of up to 5% in gas holdup occurs above this stirrer speed, depending on the liquid level and catalyst basket packing charactaristics.

- Hydrogen solubility was measured as 2.2 $^{mole}/_{m^3bar}$ at 60℃, and was found to be independent of pressure in the experimental range of 3 - 6 bar.

- Catalyst reached stable activity (according to a pseudo-first order kinetic fit) after approximately 2000 ml of liquid reagent (2% 1-octene $^{v}/_{v}$) had reacted to completion with hydrogen gas.

- Langmuir-Hinshelwood kinetics best fitted reaction data. Of the six models derived from different mechanistic postulates, the best fit (AARE = 4.6%) was obtained by the following model equation:

$$r_{OCT} = \frac{k(T)K_{OCT}C_{OCT,S}K_HC_{H_2,S}}{(1 + K_{OCT}C_{OCT,S})(1 + \sqrt{K_HC_{H_2,S}})^2} \tag{5.1}$$

Gas-limited ($\gamma = 15 - 60$) hydrogenation was carried in a 1 m long, 50 mm I.D. packed bed reactor at 60 ℃, and total pressure range of 6 - 9 bar. Packing consisted of a

9 cm section of stable catalyst (110 g) wedged between two 45 cm layers of inert allumina spheres. Main conclusions drawn from packed bed reaction studies are:

- Dry catalyst area contribution to reaction rate during downflow was not confirmed. For the two downflow modes, extensively prewetted outperformed Levec prewetted beds (known for slightly poorer wetting efficiency) for all experimental runs.
- The conventional γ-factor criterion for up-/downflow operation to predict which mode is preferable during gas or liquid reactant limiting conditions, was not sufficient to predict reactor performance for the gas-limited hydrogenation reactions. The inconsistent performance comparison of upflow vs. downflow is rather attributed to a hydrodynamic flow regime shift.
- Reactions were shown to be almost completely gas-liquid mass transfer driven, and gas-liquid mass transfer coefficients were fitted to experimental data. Downflow data was correllated with $k_{GL}a \approx 7.7\frac{P_{tot}}{M_G}v_L^{0.35}$ and $k_{GL}a \approx 8.8\frac{P_{tot}}{M_G}v_L^{0.35}$ for Levec prewetted and extensively prewetted beds respectively. No definite trend was noticed with upflow data because of an inconsistent hydrodynamic regime. The downflow correlations predicted experimental data to within 5% accuracy for runs 1 - 4.

The importance of a priori regime verification is thus emphasized. During up- downflow comparative studies it is preferable to maintain a constant flow regime, in order to investigate the effect that reactant limitations exhibit on reaction rates. Once a flow regime shift occurs, the external mass transfer rates changes accordingly, which drastically complicates the analysis.

BIBLIOGRAPHY

Al-Dahhan, M. H. and Dudukovic, M. P. (1995) "Catalyst wetting efficiency in trickle-bed reactors at high pressure", *Chemicial Engineering Science, 50* (15), 2377 – 2389.

Al-Dahhan, M. H.; Larachi, F.; Dudukovic, M. P. and Laurent, A. (1997) "High pressure trickle-bed reactors: A review", *Industrial and Engineering Chemical Research, 36*, 3292 – 3314.

Augustine, R. L.; Yaghmaie, F. and Peppen, J. F. V. (1983) "Heterogeneous catalysis in organic chemistry. 2. A mechanistic comparison of noble-metal catalysts in olefin hydrogenation", *Transactions of the Faraday Society, 49* (11), 1865 – 1870.

Banchero, M.; Manna, L.; Sicardi, S.; Boelhouwer, J. G.; Urseanu, M. I. and Kwant, G. (2004) "Conversion rate and mass transfer limitation in trickle bed reactors in the presence of a fast reaction", *Industrial and Engineering Chemistry, Process Design and Developement, 17* (3), 362 – 367.

Battsengel, B.; Datsevich, L. and Jess, A. (2002) "Experimental and theoretical studies on hydrogenation in multiphase fixed-bed reactors", *Chemical Engineering Technology, 25*, 621 – 626.

Beaudry, E. G.; Dudukovic, M. P. and Mills, P. L. (1987) "Trickle-bed reactors: Liquid diffusional effects in a gas-limited reaction", *AlChE Journal, 33* (9), 1435 – 1447.

Bressa, S. P.; Martinez, O. M. and Barreto, G. F. (2003) "Kinetic study of the hydrogenation and hydroisomerization of the n-butenes on a commercial palladium/alumina catalyst", *Industrial and Engineering Chemistry Research, 42*, 2081–2092.

Canning, A. S.; Jackson, S. D.; Monhaghan, A. and Wright, T. (2006) "C-5 alkene hydrogenation: Effect of competitive reactions on activity and selectivity", *Catalysis Today, 116*, 22 – 29.

Cassanello, M.; Larachi, F.; Laurent, A.; Wild, G. and Midoux, N. (1996) "Gas-liquid mass transfer in high pressure trickle-bed reactors: Experiments and modelling", *Process Technology Proceedings, 121*, 493 – 498.

Charpentier, J. C. (1976) "Recent progress in two phase gas-liquid mass transfer in packed beds", *The Chemical Engineering Journal, 11*, 161 – 181.

Dietriech, E.; Mathieu, C.; Delmas, H. and Jenck, J. (1992) "Raney-nickel catalyzed hydrogenations: Gas-liquid mass transfer in gas-induced stirred slurry reactors", *Chemical Engineering Science, 47*, 3597 – 3604.

Dudukovic, M. P.; Larachi, F. and Mills, P. L. (1999) "Multiphase reactors - revisited", *Chemical Engineering Science, 54*, 1975 – 1995.

Dudukovic, M. P.; Larachi, F. and Mills, P. L. (2002) "Multiphase catalytic reactors - a perspective on current knowledge and future trends", *Catalysis reviews, 44* (1), 123 – 246.

Ellman, M. J.; Midoux, N.; Laurent, A. and Charpentier, J. C. (1988) "A new, improved pressure drop correlation for trickle bed reactors", *Chemicial Engineering Science, 43* (8), 2201 – 2206.

Florusse, L. J. and Peters, C. J. (2003) "Solubility of hydrogen in heavy n-alkanes: experiments and saft modeling", *AlChE Journal, 49* (12), 3260 – 3269.

Fogler, H. S. (2006) *Elements of Chemical Reaction Engineering*, Pearson Education, Massachusetts, United States.

Gianetto, A. and Specchia, V. (1992) "Trickle-bed reactors: State of art and perspectives", *Chemical Engineering Science, 47* (13), 3197 – 3213.

Goto, S.; Chatani, T. and Matouq, M. H. (1993) "Hydrytion of 2-methyl-2-butene in gas-liquid cocurrent upflow and downflow reactors", *The Canadian Journal of Chemical Engineering, 71*, 821 – 823.

Goto, S. and Mabuchi, K. (1984) "Oxidation of ethanol in gas-liquid cocurrent upflow and downflow reactors", *The Canadian Journal of Chemical Engineering, 62*, 865 – 868.

Goto, S. and Smith, J. M. (1975) "Trickle-bed reactor performance", *AlChE Journal, 21* (4), 706 – 713.

Holah, D. G.; Hoodless, I. Y. I.; Hughes, A. N. and Sedor, L. (1979) "Kinetics of liquid-phase hydrogenation of 1-alkenes over a partially hydrogenated nickel boride and the

effect of catalyst poisons upon these hydrogenations", *Journal of Catalysis, 60*, 148 – 155.

Horiuti, I. and Polanyi, M. (1934) "Exchane reactions of hydrogen on metallic catalysts", *Transactions of the Faraday Society, 30*, 1164 – 1172.

Illiuta, I.; Ortiz-Arroyo, A.; Larachi, F.; Grandjean, B. P. A. and Wild, G. (1999) "Hydrodynamics and mass transfer in trickle-bed reactors: an overview", *Chemicial Engineering Science, 54*, 5329 – 5337.

Joubert, R. and Nicol, W. (2009) "Multiplicity behaviour of trickle flow liquid-solid mass transfer", *AlChE Journal, 48* (18), 8387 – 8392.

Khadilkar, M. R.; Wu, Y. X. and Dudukovic, M. H. A.-D. M. P. (1996) "Comparison of trickle-bed and upflow reactor performance at high pressure: Model predictions and experimental observations", *Chemical Engineering Science, 51* (10), 2139 – 2148.

Kundu, A. and Nigam, K. D. P. (2003) "Catalyst wetting characteristics in trickle-bed reactors", *AIChE Journal, 49* (9), 2253 – 2263.

Kundu, A.; Saroha, A. K. and Nigam, K. D. P. (2001) "Liquid distribution studies in trickle-bed reactors", *Chemical Engineering Science, 56*, 5963 – 5967.

Larachi, F.; Laurent, A.; Wild, G. and Midoux, N. (1992) "Pressure effects on gas-liquid interfacial areas in cocurrent trickle-flow reactors", *Chemical Engineering Science, 47* (9 - 11), 2325 – 2330.

Loudon, D.; van der Merwe, W. and Nicol, W. (2006) "Multiple hydrodynamic states in trickle flow: Quantifying the extent of pressure drop, liquid holdup and gasliquid mass transfer variation", *Chemical Engineering Science, 61*, 7551 7562.

Mazzarino, I.; Occhetti, M.; Baldi, G. and Sicardi, S. (1989) "Performance of a packed-bed reactor with a two phase upward flow", *Chemical Engineering Communication, 75*, 225 – 240.

Meille, V.; de Bellefon, C. and Schweich, D. (2002) "Kinetics of α-methylstyrene hydrogenation on Pd/Al_2O_3", *Industrial and Engineering Chemistry Research, 41*, 1711 – 1715.

Metaxas, K. C. and Papayannakos, N. G. (2006) "Kinetics and mass transfer of benzene hydrogenation in a trickle-bed reactor", *Industrial and Engineering Chemistry Research, 45*, 7110 – 7119.

Mitrovic, M.; Pitault, I. and Forissier, M. (2005) "Liquid-solid mass transfer in a three-phase stationary catalytic basket reactor", *AlChE Journal, 51* (6), 1747 – 1757.

Molga, E. J. and Westerterp, K. R. (1997) "Gas-liquid interfacial area and holdup in cocurrent upflow packed bubble column reactor at elevated pressures", *Industrial and Engineering Chemistry Research, 36*, 622 – 631.

Monteiro-Gezork, A. C. A.; Natividad, R. and Winterbottom, J. M. (2008) "Hydrogenation of naphthalene on NiMo-, Ni- and Ru/Al_2O_3 catalysts: LangmuirHinshelwood kinetic modelling", *Catalysis Today, 130*, 471 – 485.

Murugesan, T. and Sivakumar, V. (2002) "Pressure drop and flow regimes in cocurrent gasliquid upflow through packed beds", *Chemical Engineering Journal, 88*, 233 – 243.

Pitault, I.; Fongarland, P.; Koepke, D.; Mitrovic, M.; Ronze, D. and Forissier, M. (2005) "Gas-liquid and liquid-solid mass transfers in two types of stationary catalytic basket laboratory reactor", *Chemical Engineering Science, 60*, 6240 – 6253.

Reiss, L. P. (1967) "Cocurrent gas-liquid contacting in packed columns", *Chemical Engineering Progress, 50* (8), 396 – 4028.

Roininen, J.; Alopaeus, V.; Toppinen, S. and Aittamaa, J. (2009) "Modeling and simulation of an industrial trickle-bed reactor for benzene hydrogenation: Model validation against plant data", *Industrial and Engineering Chemistry Research, 48*, 1866 – 1872.

Sarkar, A.; Seth, D.; Ng, F. T. T. and L, R. G. (2006) "Kinetics of liquid-phase hydrogenation of isooctenes on a Pd/γ-Alumina catalyst", *American Institute of Chemical Engineers, 52* (3), 1142 – 1156.

Satterfield, C. N. (1975) "Trickle-bed reactors", *AlChE Journal, 21* (2), 210 – 228.

Specchia, G.; Baldi, G. and Gianetto, A. (1978) "Solid-liquid mass transfer in concurrent two-phase flow through packed beds", *Chemical Engineering Science, 59*, 5411 – 5416.

Sylvester, N. D. and Pitayaguisarn, P. (1975) "Mass transfer for two-phase cocurrent downflow in a packed bed", *Industrial and Engineering Chemistry, Process Design and Developement, 14* (4), 421 – 426.

Toppinen, S.; Rantakyla, T.; Salmli, T. and Aittamaa, J. (1997) "The liquid phase hydrogenation of benzene and substituted alkylbenzenes over a nickel catalyst in a semi-batch reactor", *Catalysis Today, 38*, 23 – 30.

Trambouze, P. and Euzen, P. (2004) *Chemical Reactors*, Editions Technip – Paris, France.

Uchytil, J.; Jackubickova, E. and Kraus, M. (1979) "Hydrogenation of alkenes over a cobalt-molybdenum-alumina catalyst", *Journal of Catalysis, 64*, 143 – 149.

van der Merwe, W. and Nicol, W. (2008) "Effect of hydrodynamic multiplicity on trickle bed reactor performance", *AlChE Journal, 54* (10), 249 – 257.

van Houwelingen, A. (2009) "Liquid-solid contactng in trickle-bed reactors", *Ph.D Thesis,* pages 1 – 96.

van Houwelingen, A. and Nicol, W. (2009) "Parallel hydrogenation for the quantification of wetting efficiency and liquid-solid mass transfer in a trickle-bed reactor", *AlChE Journal, Article in press* (DOI - 10.1002/aic.12342).

van Houwelingen, A. J.; Kok, S. and Nicol, W. (2009) "Effectiveness factors for partially wetted catalysts", *AlChE Journal, Article in press* (10.1021/ie9017176).

van Houwelingen, A. J.; Sandrock, C. and Nicol, W. (2006) "Particle wetting distributions in trickle bed reactors", *AlChE Journal, 52* (10), 3532 – 3542.

van Krevelen, D. W. and Krekels, J. T. C. (1948) "Rate of dissolution of solid substances", *Recueil Des Travaux Chimiques, 67*, 510 – 515.

Vannice, V. and Singh, U. (2001) "Kinetics of liquid-phase hydrogenation reactions over supported metal catalysts - a review", *Applied Catalysis, 213*, 1 – 24.